ELSEVIER

Contents lists available at ScienceDirect

Cold Regions Science and Technology

journal homepage: www.elsevier.com/locate/coldregions



Synthesis of physical processes of permafrost degradation and geophysical and geomechanical properties of permafrost

Min Liew ^{a,*}, Xiaohang Ji ^a, Ming Xiao ^a, Louise Farquharson ^b, Dmitry Nicolsky ^b, Vladimir Romanovsky ^b, Matthew Bray ^c, Xiong Zhang ^d, Christopher McComb ^e

- ^a Department of Civil and Environmental Engineering, The Pennsylvania State University, University Park, PA 16802, United States
- ^b Geophysical Institute, University of Alaska Fairbanks, Fairbanks, AK 99775, United States
- ^c Department of Civil and Environmental Engineering, University of Alaska Fairbanks, Fairbanks, AK 99775, United States
- d Department of Civil, Architectural and Environmental Engineering, Missouri University of Science and Technology, MO 65409, United States
- e Mechanical Engineering, Carnegie Mellon University, Pittsburgh, PA 15213, United States

ARTICLE INFO

Keywords: Permafrost Degradation Frozen soil Geophysical Geomechanical Geotechnical

ABSTRACT

Recent permafrost degradation across the high northern latitude regions has impacted the performance of the civil infrastructure. This study summarizes the current state of physical processes of permafrost degradation in a geotechnical context and the properties of permafrost-affected soils critical for evaluating the performance of infrastructures commonly built in the high northern latitude regions. We collected a total of 96 datasets with 3162 data points from 38 journal and conference publications and analyzed the variations of geomechanical and geophysical properties under the effects of permafrost degradation. The datasets represent a range of geomechanical and geophysical properties of permafrost-affected soils with different compositions under different testing conditions. While the data collected are highly scattered, regression analysis shows that most geomechanical and geophysical properties have strong associations with temperature. These associations highlight that ongoing warming can greatly affect the performance of civil infrastructures at high northern latitudes. These properties include elastic moduli, strength parameters, thermal conductivity, heat capacity, unfrozen water content, and hydraulic conductivity. This paper also discusses other factors, such as soil type, soil composition, and confining pressure, which may further complicate the relationships between temperature and the geomechanical and geophysical properties. Through this review, we identify key knowledge gaps and highlight the complex interplay of permafrost degradation, temperature, soil heterogeneity, and soil geomechanical and geophysical properties. Given the scarcity of certain permafrost properties in addition to the complex processes of permafrost degradation in the geotechnical context, there is a need to establish a comprehensive and curated database of permafrost properties. Hence, we encourage broader collaboration and participation by the engineering and scientific communities in this effort.

1. Introduction

The ground in northern high latitudes within the regions with continuous permafrost distribution consists of two layers: permafrost and the active layer. Permafrost is ground that remains at or below 0 $^{\circ}$ C for at least two consecutive years, whereas the active layer, which is underlain by permafrost, is the near-surface layer that freezes in the winter and thaws in the summer. Historically, permafrost has served as a strong foundation for civil infrastructure in the northern high latitudes.

In regions where the permafrost table is shallow, end-bearing piles can be driven into the permafrost, providing an adequate bearing capacity for structures (Rice, 1972; Nash and Carlson, 2015). Although the active layer thaws during summer months each year and loses strength, the performance of deep foundations will not be affected if permafrost is still stable. This is because the structural loads are transmitted to and supported by the permafrost, which remains frozen even in the summer. Rising air temperatures, however, are driving permafrost degradation in high-latitude regions (Jorgenson et al., 2006; Romanovsky et al., 2010;

E-mail addresses: mul393@psu.edu (M. Liew), xbj5039@psu.edu (X. Ji), mzx102@psu.edu (M. Xiao), lmfarquharson@alaska.edu (L. Farquharson), djnicolsky@alaska.edu (D. Nicolsky), veromanovsky@alaska.edu (V. Romanovsky), mtbray@alaska.edu (M. Bray), zhangxi@mst.edu (X. Zhang), ccm@cmu.edu (C. McComb).

^{*} Corresponding author at: Department of Civil and Environmental Engineering, 212 Sackett Building, The Pennsylvania State University, University Park, PA 16802-1408, United States.

Biskaborn et al., 2019). As a result, the performance of civil infrastructure is being affected by various modes of permafrost degradation such as permafrost warming (Nelson et al., 2002; Olsen, 2015), active layer thickening (Anisimov et al., 1997; Osterkamp and Romanovsky, 1999; Osterkamp, 2007; Rowland et al., 2010), and talik formation (Smith and Riseborough, 2010).

Ongoing climate warming and subsequent permafrost degradation is expected to have widespread negative impacts on infrastructure (Nelson et al., 2001; Melvin et al., 2016; Hjort et al., 2018). Nelson et al. (2001) quantified the risks of permafrost subsidence under climate change in the northern hemisphere and delineated high-risk areas to which high priority should be assigned for high-resolution monitoring at a resolution of 0.5° latitude/longitude. Larsen et al. (2008) predicted that permafrost degradation will raise the maintenance cost of public infrastructure by \$3.6-\$6.1 billion by 2030 and another \$5.6-\$7.6 billion by 2080 in Alaska. Melvin et al. (2016) predicted that the cumulative costs of climate-related damages to Alaskan infrastructure from 2015 to 2099 to be \$5.5 billion for Representative Concentration Pathway (RCP) 8.5 (representing the highest greenhouse gas emissions scenario projected by the Intergovernmental Panel on Climate Change (IPCC)) and \$4.2 billion for RCP 4.5 (representing stabilizing greenhouse gas emissions scenario). Under RCP 4.5, Hjort et al. (2018) estimated that 69% of the infrastructure in the Arctic will be at high risk of near-surface permafrost thaw by 2050 and 33% of the infrastructure will be severely damaged due to the substantial ground subsidence and loss of bearing capacity. All the aforementioned studies agreed that projected climate change could put Arctic infrastructure and residents at risk and impose high repair and maintenance costs.

Besides geologic hazards and structural damage, the societal impacts of permafrost degradation are also recognized in the literature with topics ranging from community relocation (Shearer, 2012; Marino, 2012; Bronen and Chapin, 2013; Maldonado et al., 2013; Bronen, 2015) to cultural heritage preservation (Hollesen et al., 2018; Marsadolov et al., 2019), and community resilience (Ford et al., 2007; Bronen et al., 2019). Although these are not the focus of this paper, the understanding and prediction of how permafrost and infrastructure's foundations behave under climate change are relevant to such discussions. As a result, the U.S. Arctic Research Commission Permafrost Task Force (2003) recommended the development of design criteria specifically for permafrost-influenced infrastructure and the initiation of more studies oriented to permafrost engineering applications.

For the past several decades, there have been several reviews and syntheses of the mechanical behaviors of frozen soils. Stress-strain relationships of frozen soils under various testing conditions (e.g., confining stress, strain rate, and temperature) were summarized by Ladanyi (1981) based on the research advancement in 1970-1980. Razbegin et al. (1996) reviewed the mechanical properties of frozen soils at subzero temperatures and discussed the factors that affect mechanical behavior, including loading regime, types of stress state, microstructures, testing methods, intrinsic properties, and boundary conditions. Jessberger (1981) synthesized the design procedures of ground freezing techniques and the mechanical properties of artificially frozen soil. Qi et al. (2006) reviewed how geotechnical properties are affected by freeze-thaw cycles. Reviews of the creep behavior of frozen soils can be found in Ladanyi (1972), Ting (1983), Arenson et al. (2007), and Qi et al. (2013). While these reviews provided in-depth discussions of the mechanical behavior of frozen soils and their governing factors, many discussions were qualitative, and syntheses may not be directly applicable to quantitative modeling efforts, which aimed at evaluating the performance of infrastructure influenced by permafrost degradation.

The strength and deformation of degrading permafrost depend on its soil composition, boundary conditions, and environmental forcing factors. However, soil temperature is often regarded as the major factor affecting the geomechanical and geophysical properties of permafrost-affected soils and influencing the degree of permafrost degradation. For this reason, this paper focuses on quantifying the variations of

geomechanical and geophysical properties of permafrost-affected soils with temperature and detailing the soil compositions and testing conditions for each dataset. Only the geophysical and geomechanical properties of permafrost-affected soils that are relevant to evaluating the effects of permafrost degradation on civil infrastructure are selected in this study. In this paper we (1) summarize the physical processes of permafrost degradation in a geotechnical context, (2) summarize permafrost and frozen soil properties that are essential for evaluating the impacts of permafrost degradation on foundation performance, (3) conduct a meta-analysis on the collected soil properties, (4) analyze how the properties vary during permafrost degradation and how the variations are affected by other factors, and (5) identify knowledge gaps that hinder cold region engineers and scientists from quantifying foundation performance affected by degrading permafrost. The goal of this research is to provide a comprehensive overview and generate new quantitative knowledge of geophysical and geomechanical characteristics of degrading permafrost so that the knowledge can be used to evaluate the foundations of civil infrastructure in the changing Arctic.

2. Physical processes of permafrost degradation in a geotechnical context

The physical response of permafrost-affected soils to climate warming depends on the complex interplay between increases in air temperature, changes in precipitations, the ground thermal regime, excess ice content, and soil composition. Fig. 1 depicts a permafrost degradation model schematic, which consists of changes in ground thawing and freezing processes. Processes that occur during ground thawing are #1) inflow of heat energy, #2) reduction in soil strength, #3) water migration, #4) ground settlement. Processes that occur during freeze are #5) outflow of heat energy, #6) migration of water to the freezing front, #7) frost heaving, and #8) an increase in soil strength. Ongoing warming is currently causing thaw-driven cumulative settlement and strength reduction in permafrost. Both freezing and thawing processes occur in active layer or newly formed active layer, which used to be permafrost before affected by climate warming.

2.1. Physical processes of permafrost thawing

As shown in Fig. 1, thawing of the active layer and permafrost can be described by the following four processes that occur simultaneously: (1) inflow of heat energy, (2) reduction of soil strength, (3) water migration, and (4) ground settlement. The inflow of heat energy (process #1) is initiated by an increase in near-surface air temperature and a subsequent increase in ground surface temperature. The heat energy exchange between the near-surface atmosphere and the ground surface is affected by surface characteristics such as vegetation and snow cover (Luo et al., 2018). However, this study only focuses on the heat transfer process in the soil domain. During this process, heat is transferred from the ground surface into the soil domain through thermal conduction and in some cases through occasional thermal convection due to groundwater percolation, resulting in changes in temperature of the active layer and permafrost. Heat energy is used as the latent heat of fusion to melt not only some ice at the thaw front, but also some interstitial ice and hence increase unfrozen water content in the near-surface permafrost (Nicolsky and Romanovsky, 2018). Unfrozen water can exist even when the temperature is below 0 °C, and its content can increase with temperature (Williams, 1964; Anderson and Tice, 1972; Romanovsky and Osterkamp, 2000). The increase in unfrozen water content in both the active layer and upper permafrost leads to a reduction in ice adhesion (Jessberger, 1981; Arenson et al., 2007), causing the shear strength of soil to decrease (process #2). Even for compacted soil, the shear strength highly depends on the liquid water content and thus can be reduced by up to 50% at the onset of thawing (De Guzman et al., 2018). Upon melting of pore ice, part of the overburden load initially supported by the ice matrix is transferred to pore water, causing the pore water

Physical Processes and Modeling of Permafrost Degradation

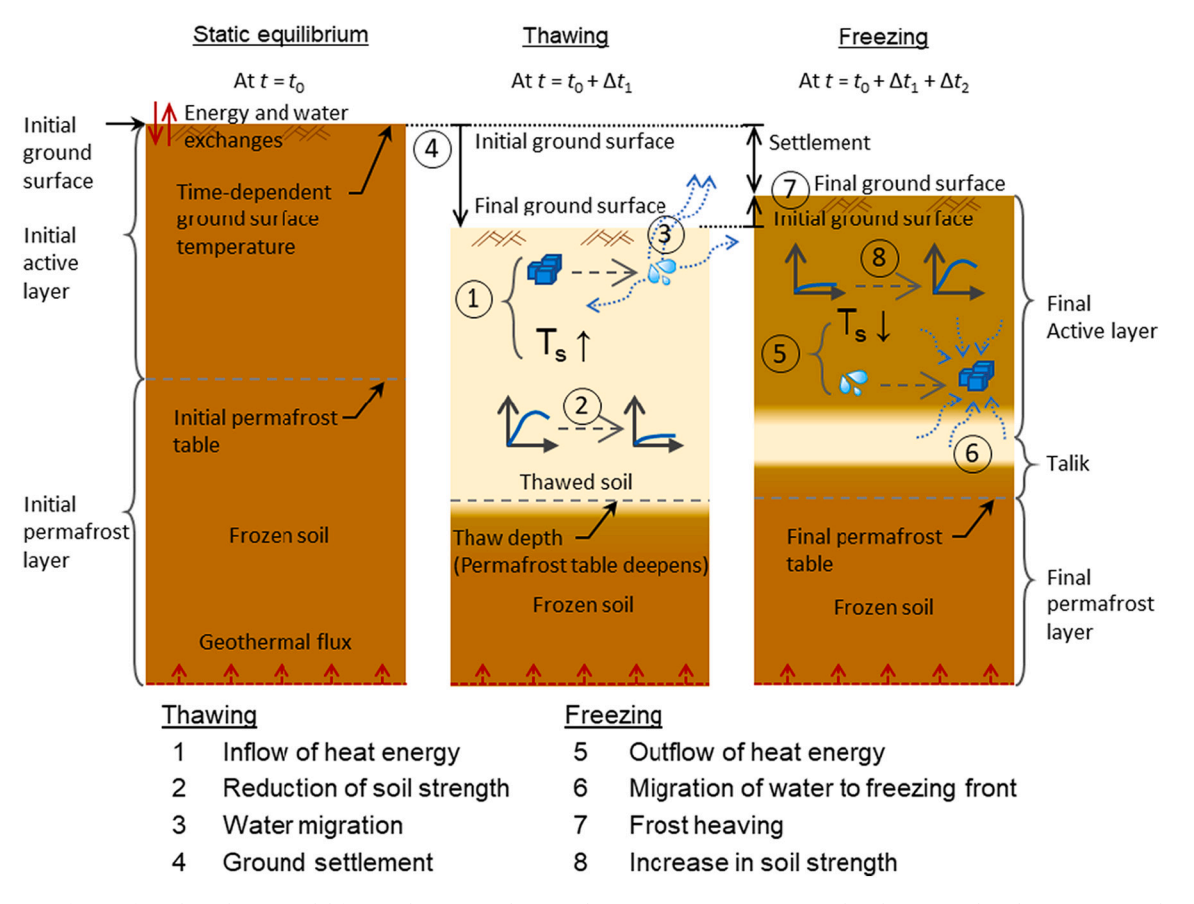


Fig. 1. Schematic of permafrost degradation model for simulating cumulative soil temperature increase, strength reduction, and settlement. ($T_s = \text{soil}$ temperature).

pressure to increase (Morgenstern and Nixon, 1971; Dumais and Konrad, 2018). This excess pore water pressure coupled with an increase in hydraulic conductivity (which depends on the liquid water content) in the thawed soil initiates process #3, during which excessive water flows out of the system. Dissipation of excess pore water pressure leads to transfer of the overburden load to the soil skeleton, resulting in an increase in the vertical effective stress and a reduction in void ratio. The thaw consolidation and subsequent ground settlement, as defined in process #4, are dominant contributors to soil deformation during thawing (Morgenstern and Nixon, 1971; Dumais and Konrad, 2018). They account for approximately 40% reduction in soil thickness for ice-rich fine-grained soil (Andersland and Ladanyi, 2004) and are more significant than the 9% volumetric reduction due to phase change of ice to water.

2.2. Physical processes of soil freezing

Active layer refreezing during the winter months can be described by the following processes (Fig. 1): the outflow of heat energy (process #5), migration of water to the freezing front (process #6), frost heaving (process #7), and increase in soil modulus and strength (process #8). During process #5, heat flows out of the ground surface and subsequently its temperature decreases. As a result, heat in the soil domain gradually redistributes through thermal conduction, resulting in a decrease in temperature for the entire soil domain. At the freezing point of water, part of the pore water changes to pore ice, and latent heat of fusion is released. The phase change of water near the ground surface and permafrost table leads to process #6. In this process, a freezing front parallel to the ground surface (or perpendicular to the heat flow) starts to develop, and pore water moves from the unfrozen soil elements

towards the freezing front (i.e., in the direction of lower temperature) due to the hydraulic head difference caused by a temperature gradient under a uniform pressure field (Hoekstra, 1966; Mageau and Morgenstern, 1980). This is known as cryogenic suction. Another freezing front occurs at the top of permafrost and at the base of the active layer, leading to migration of water towards the permafrost table albeit at a slower pace. In process #7 (frost heaving), as water continues to flow towards the freezing front, water expands upon freezing, and ice forms and segregates the soil grains, causing soil porosity to increase and the soil to heave. However, the growth of ice lenses is gradually impeded when the latent heat, which is released through a phase change, reduces the thermal gradient and water seepage towards the freezing front (Rempel, 2007). The extent of ice segregation is also restricted by the overburden stress (Rempel, 2007).

In process #8, as part of the pore water changes to pore ice, ice adhesion increases (Jessberger, 1981; Arenson et al., 2007), resulting in an overall increase in the modulus and shear strength of the soil. It is important to note that the modulus and shear strength of soil varies with depth during the freezing process. Such variation is owing to the dominant top-down refreeze from the ground surface and an upward refreeze from the permafrost table. This bidirectional freezing results in a three-layer active layer: a bottom frozen layer, an intermediate unfrozen layer, and an upper frozen layer. During ice segregation, water flows out of the unfrozen layer and moves towards the freezing front, causing the unfrozen layer to consolidate (Hui and Ping, 2009; Zhang et al., 2016). As soil consolidates, its void ratio reduces, causing an increase in shear strength (as compared to the shear strength of the thawed soil before consolidation) in the unfrozen layer. In the frozen layers, the phase change causes ice adhesion to increase, resulting in higher shear

strength (Jessberger, 1981; Arenson et al., 2007). However, as ice segregates and ice lenses form in the frozen layers, the ratio of the mass of soil grains to the mass of ice per unit volume decreases, causing the shear strength of this layer to be slightly less than its shear strength before ice segregation (Andersland and Ladanyi, 2004). Nonetheless, the overall shear strength significantly increases.

2.3. Modes of permafrost degradation and features that amplify the degradation

Without climate change, permafrost-affected soils thaw and freeze with natural variations in air temperature. Freeze-thaw cycles are limited to the active layer since permafrost remains frozen all year long. As climate warms, the ground thermal regime changes and permafrost warms up. Even when the warming of permafrost occurs below the freezing point of pure water, unfrozen water content increases in permafrost because of the freezing point depression due to the cumulative effect of pore water salinity, pore water pressure, and fines content (Collett and Bird, 1988). As the ground temperature in the upper permafrost increases above 0 °C in the summer months, the freeze-thaw cycles extend beyond the original active layer and into the previously stable permafrost layer. This extension of seasonal freeze-thaw is known as the thickening of active layer and is one of the reasons for civil infrastructure failures in northern high-latitude regions. The thawing and freezing processes of this newly formed active layer are the same as those previously described in Fig. 1. For a while, a new active layer typically refreezes completely in the winter months. If there is an incomplete top-down refreeze, an unfrozen layer will persist through the winter months. This year-round unfrozen layer is known as a talik (Parazoo et al., 2018). It is further classified as a closed talik if enclosed within two frozen layers in the winter. Essentially, permafrost degradation can be categorized into three modes: (1) warming of permafrost below the freezing point of water without changes in active layer thickness, (2) active layer thickening, and (3) talik development. These degradation modes can shorten the service life and increase the maintenance cost of civil infrastructure. They are typically due to either a disturbance of the ground surface (e.g., due to removal of vegetation by humans, wildfire, or infrastructure construction), or an increase in snow depth or air temperature because of climate change.

The changing ground thermal regime greatly affects the performance of civil infrastructure. Such effects are often amplified by periglacial features such as ground ice. Compared to ice-poor sites, sites with excess ground ice have a high potential for severe ground subsidence (Williams and Smith, 1989; Hjort et al., 2018). Melting of ice wedges and thick ice lenses at these sites also leads to ponding beneath residences, posing drowning hazards to young children (personal communication with Point Lay residents, February 2020). At coastal or riverine sites, the effects of permafrost degradation are often exacerbated by water actions. Rapid erosion processes unique to ice-rich permafrost coasts and riverbanks include thermal abrasion, thermal denudation, and thermal settling (Aré, 1988; Hoque and Pollard, 2009, 2016). Thermal settling and abrasion are due to the thermal action or combined mechanical and thermal action of water, respectively, while thermal denudation is the destruction of shore cliffs of thermoabrasional coasts under the action of thermal energy of air and solar radiation (Aré, 1988; Liew et al., 2020). As such, thermal denudation can be regarded as the coast- or bankspecific permafrost degradation, which can sometimes be amplified by abrasion. Permafrost degradation and coastal or riverine erosion are often interrelated. As noted in Overduin et al. (2014), deeper terrestrial permafrost that persists below the level of coastal erosion may become subsea permafrost if the shoreline continues to migrate landward. This means that degraded inland permafrost, albeit located away from the coastline, may further contribute to the ongoing land loss. In such cases, the civil infrastructure there is no longer serviceable.

3. Geomechanical and geophysical characteristics of permafrost-affected soils for *evaluating* performance of civil infrastructure under permafrost degradation

Permafrost-affected soil exists in an extreme environment and is subjected to various environmental forcing factors. Even when the variability of the forcing factors is neglected, the modeling of permafrost-affected soil is still challenging given that the soil itself is highly heterogeneous in terms of its physical constituents, geophysical characteristics, and geomechanical characteristics. Table 1 identifies the challenges of site selections and civil infrastructure designs under the impacts of permafrost degradation. Based on the synthesis of physical processes (Fig. 1), challenges (Table 1), and studies related to the constitutive modeling for frozen soils (Thomas et al., 2009; Hoque and Pollard, 2009, 2016; Yamamoto, 2013; Zhang and Michalowski, 2015; Kadivar and Manahiloh, 2019), the following properties are important

 Table 1

 Challenges of site selections and civil infrastructure designs under the impacts of permafrost degradation.

Challenges	Descriptions	References
Settlement	 Warming of an ice bearing permafrost body at depth Increased seasonal thaw depth Talik development in ice-bearing permafrost Settlement or subsidence due to soil compaction due to meltwater expulsion from thawing ice-bearing permafrost 	 Allard et al., 2012 Olsen, 2015
Coastline- and riverbank- related degradation	 Block failure Thermal erosion and denudation 	 Aré, 1988 Hoque and Pollard, 2009, 2016 Liew et al., 2020
Slope instability	 Retrogressive thaw slump Landslide due to increase of pore water pressure caused by meltwater expulsion from thawing permafrost 	■ Lantuit and Pollard, 2008 ■ Costard et al., 2021 ■ Olsen, 2015 ■ Allard et al., 2012 ■ Yamamoto, 2013
Damage to deep foundations	 Increased frost heave effect on piles Reduced bearing capacity Slow freeze-back rate of soil-pile interface Settlement in plastic frozen soil and ice-rich soil Thaw settlement Reduced adfreeze bond for pilings Decrease in the effective length of piling in permafrost 	 Morgenstern, 1983 Weaver and Morgenstern, 1981 Olsen, 2015 Allard et al., 2012 Vyalov, 1983 Ding, 1983
Damage to road and railway embankment	 Thaw settlement Frost heave Increased temperature variation at embankment slope 	Tian et al., 2019Esch, 1983Olsen, 2015
Damage to water- retaining embankment	 Increased seepage Increased erosion Structural instability Increased thermal and mechanical erosion (piping) 	■ Morgenstern, 1983 ■ Sayles, 1983

in modeling the critical processes of permafrost degradation:

- (1) Change in settlement or heaving and bearing capacity: Young's modulus (E), bulk modulus (K), Poisson's ratio (ν), shear modulus (G), shear wave velocity (V_s), compressional wave velocity (V_p), friction angle (φ), cohesion (c), compressive strength, and tensile strength:
- (2) Hydraulic conductivity (k_w) and unfrozen water content (w_u);
- (3) Heat transfer: thermal conductivity (k_h) and volumetric heat capacity (c_h) .

4. Meta-analysis of data collection

In this paper, we collected a total of 96 datasets with 3162 total data points from 38 journal and conference publications for analyzing the variations of geomechanical and geophysical properties under the effects of permafrost degradation. The datasets represent a range of geomechanical and geophysical properties of permafrost-affected soils with various soil types and soil compositions under various testing conditions. The number of data points (n) for each soil property is illustrated in Fig. 2a, and the number of data points for each soil type is shown in Fig. 2b. The meta-analysis indicates that unfrozen water content (n =1465 or 39%) is the most tested property, followed by elastic moduli (n = 771 or 20%), and thaw strain (n = 648 or 17%). Heat transfer property, shear strength parameter, maximum deviatoric stress, and hydraulic conductivity are the least tested ones (n < 300 in all cases). Unfrozen water content is the most tested property since it influences the degree of permafrost degradation and is responsible for the variations in geomechanical properties with temperature. Based on the data collected in this study, fine-grained soil (n = 2205 or 70%) is the most tested soil type, followed by sand with fines (n = 425 or 13%) and sand (n = 361 or 11%). Fine-grained soil is most tested, which is probably due to its capability to hold more moisture, and therefore is more susceptible to permafrost degradation. Organic soil and gravel are the least tested soil types. Soils are classified using the Unified Soil Classification System (USCS). Given that the focus of this paper is permafrost degradation (i.e., temperature change), the temperature distribution of the tested soil samples is presented in Fig. 3. The zoom-in chart in Fig. 3 has more increments within temperatures ranging from -5 to 0 °C, showing a

more detailed temperature distribution within this critical temperature range. Most of the soil samples were tested at temperatures near 0 $^{\circ}\text{C}.$ This is because the geomechanical and geophysical properties of permafrost are likely to change dramatically near 0 $^{\circ}\text{C}.$

Index properties of the tested soils, including gravimetric and volumetric moisture contents, porosity, bulk density (i.e., the ratio of the total mass of soil grains and moisture to the total volume of the soil), and dry density (i.e., the ratio of the mass of soil grains to the total volume of the soil) were statistically analyzed. The variations of these properties with soil types are presented in Fig. 4a—e with outliers shown as rhombus markers. Based on the analysis, organic soil and silt have the highest median moisture content (both gravimetric and volumetric) (Fig. 4a—b) and the highest median porosity (Fig. 4c). Correspondingly, organic soil and silt have the lowest median bulk density and dry density (Fig. 4d—e). Coarse-grained soils, which include gravel, sand, and sand with fines, have the lowest median gravimetric and volumetric moisture contents and median porosity, while their median bulk density and dry density are the highest. Clays are in the middle of the range.

5. Statistical method for analyzing the variations

Regression analysis is used to understand the relationships of various properties with temperature. For nonlinear relationships, the values of the influence factors (i.e., temperature, total moisture content) and the geomechanical and geophysical properties are transformed to linearize the relationships. P-values are then generated for the transformed relationships to evaluate whether the geophysical and geomechanical properties are strongly associated with the chosen factors. The P-value represents the marginal significance level of a statistical hypothesis test. A P-value of less than 0.005 constitutes a statistical evidence for the linear association of two parameters at the 99.5% confidence level. Table 2 summarizes the P-values for the relationships between the geomechanical and geophysical properties and their possible influence factors. A relationship with a strong statistical association (i.e., P-value < 0.005) between a property and its possible influence factor is labelled "Y"; a relationship with a weak or no association is labelled "N." Based on the collected data, Table 2 provides a quantitative overview of factors that may influence the geomechanical and geophysical properties of permafrost-affected soils, and these relationships are further explored

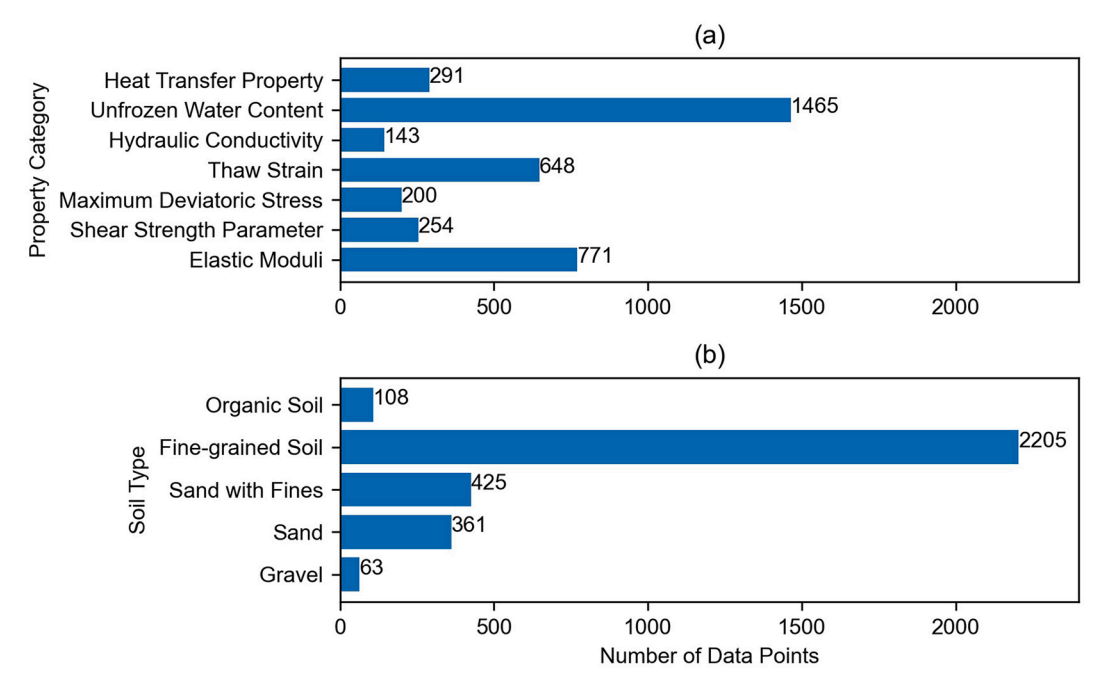


Fig. 2. Meta-analysis of the variation of geomechanical and geophysical properties under the effects of permafrost degradation.

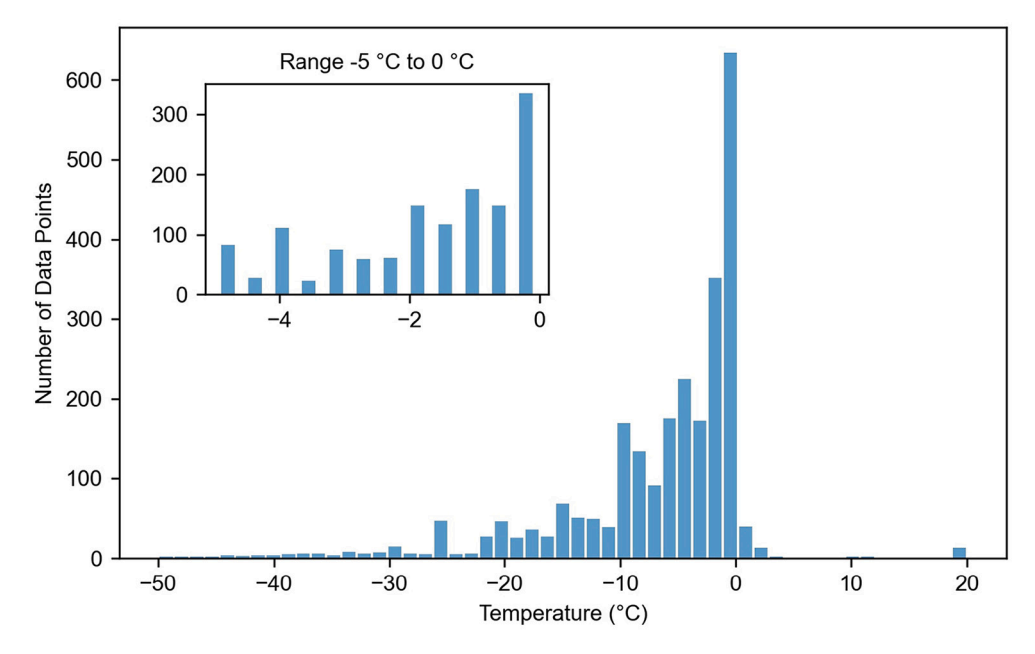


Fig. 3. Distribution of temperatures at which the geomechanical and geophysical properties of permafrost-affected soils were measured.

and explained in the subsequent sections.

6. Reduction of elastic moduli upon warming

In this study, the following elastic moduli are collected: bulk modulus (K), shear modulus (G), compressional wave velocity (V_p), shear wave velocity (V_s), Young's modulus (E), and Poisson's ratio (ν). Since other moduli can be calculated once knowing any two of these six moduli (see Eqs. (1)–(4); Mavko et al., 2003), all elastic moduli collected in this study have been converted into K and G.

$$V_p = \sqrt{\frac{K + \frac{4}{3}G}{\rho}} \tag{1}$$

$$V_s = \sqrt{\frac{G}{\rho}} \tag{2}$$

$$E = \frac{9KG}{3K + G} \tag{3}$$

$$\nu = \frac{3K - 2G}{2(3K + G)} \tag{4}$$

where V_p is compressional wave velocity, V_s is shear wave velocity, E is Young's modulus, ν is Poisson's ratio, K is bulk modulus, G is shear modulus, and ρ is the bulk density of a soil specimen.

Fig. 5a–c show the variations of bulk modulus with temperature for sand, sand with fines, and fine-grained soils, respectively. A soil specimen is defined as sand with fines when the percentage of fines is greater than 12% but less than 50%. In general, bulk moduli decrease gradually with temperature from −30 to −5 °C and then decrease rather rapidly with temperature from −5 to 0 °C. The moduli quickly reduce to zero after 0 °C. In Fig. 5a–c, the markers are color-coded with blue indicating high total moisture content and yellow indicating low total moisture content. A red marker is used when the total moisture content is not reported. Sand (in Fig. 5a) has a clearer trend of gradual transition from blue to yellow. This observation indicates that soils with higher total moisture content exhibit higher bulk modulus. This trend can be observed for sand with fines and fine-grained soils when the data by Zhang et al. (2018) are removed. The soil samples in Zhang et al. (2018) have high salinity content (5 ppt), while all other soil samples included

in Fig. 5 are non-saline soils. Because of the salinity content, the soils tested by Zhang et al. (2018) exhibit lower bulk modulus despite having higher total moisture content. Non-saline sand with fines and finegrained soils, if having higher total moisture contents, also experience a relatively sharp decrease in their modulus in the temperature range of 5–0 °C. For example, for sand with fines in Fig. 5b, the data by Li (2009) have higher total moisture contents ($w_{\text{total}} = 20\%$) and show a sharper modulus reduction near 0 °C than the data by Christ et al. (2009) (wtotal = 12%) and Kim et al. (2015) ($w_{\text{total}} = 8-11$ %). Similarly, for finegrained soils in Fig. 5c, the data by Li (2009) with higher total moisture contents ($w_{\text{total}} = 20\text{--}36\%$) also have a sharper modulus reduction near 0 °C than the data ($w_{\text{total}} = 20\%$) by Christ et al. (2009). We reason that, for sand with fines and fine-grained soils without salinity content, the soils exhibit a trend (i.e., sharper reduction of modulus near water melting temperature) closer to sand if the total moisture content is higher. This is because, for non-saline sand with fines and fine-grained soils with higher total moisture contents, the ice content reduces interactions between fine particles, causing these soils to behave more like sand. There are also some exceptions. In Fig. 5a, although having high total moisture content (30-34%), data by Li (2009) have relatively low bulk moduli when compared to data by Nakano and Arnold (1973). This is because fine sand was used in Li (2009), while medium sand was used in Nakano and Arnold (1973). The results are reasonable given that medium sand generally has higher bulk modulus than fine sand.

Boxplots comparing the bulk moduli for different soil types across different ranges of temperature are presented in Fig. 5d. The boxplots show that sand has a higher median bulk modulus than sand with fines and fine-grained soils at any given temperature within the range of -30 $^{\circ}C$ – 0 $^{\circ}C$. Although the median bulk modulus of fine-grained soil is slightly greater than that of sand with fines at a certain temperature range, the difference is not significant and could be due to data bias. In Fig. 5c, the bulk moduli of fine-grained soils measured by Lee et al. (2002) range from 9 to 35 GPa at -10 °C. This significant variation of bulk modulus under the same temperature is due to the variation of soil density. Lee et al. (2002) reported that the bulk moduli of these soil specimens measured at $-10\,^{\circ}\text{C}$ increase with increasing relative density. The bulk moduli presented in Fig. 5 are obtained mostly using ultrasonic tests with frequency ranging from 400 kHz to 2 MHz. Kim et al. (2015) determined the moduli using resonant column, Lee et al. (2002) used hydrostatic compression tests, and Zhang et al. (2018) used bender

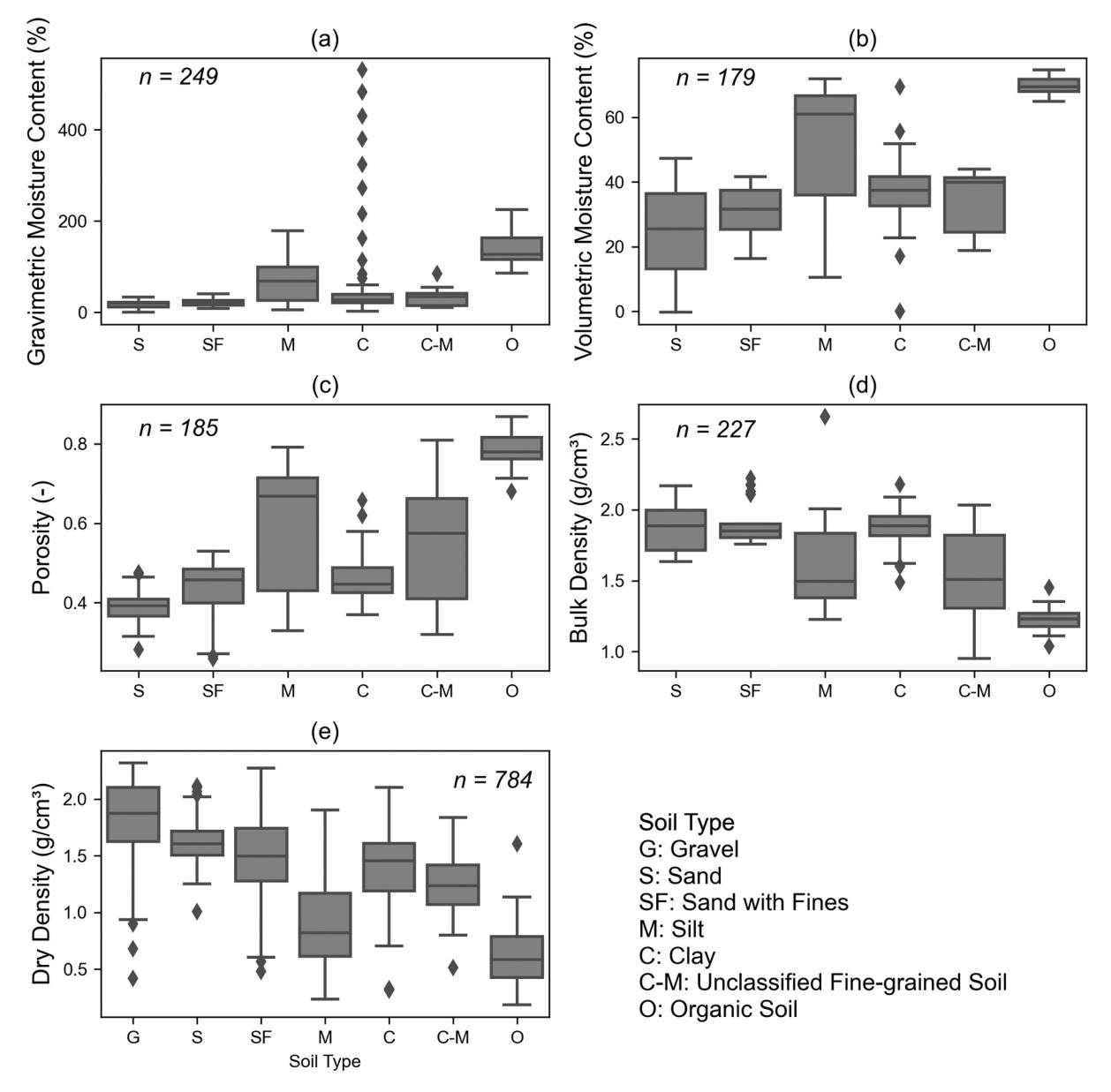


Fig. 4. Boxplots of index properties: (a) gravimetric moisture content, (b) volumetric moisture content, (c) porosity, (d) bulk density, and (e) dry density. The sample size, *n*, of each property is listed in each subfigure. The rhombus markers represent the outliers.

element and bending disk tests. Nevertheless, this study focuses on the influences of temperature, soil compositions, and soil type, therefore deviations in the moduli due to testing methods are not further explored. Details regarding the testing methods and conditions can be referred to the supplementary materials.

Regression analyses are performed to assess the influence of various factors on bulk modulus. The regression analysis shows that bulk modulus is linearly associated with the natural logarithm of temperature for all soil types with *P*-value less than 0.005 (Table 2). On the other hand, the regression analysis based on the collected data shows that bulk modulus is not associated with total moisture content for fine-grained soil regardless of the inclusion of data points of saline permafrost. Bulk modulus measures how a material response to uniform compression. Ice matrix due to the increase in total moisture content helps the sandy soil specimens resist the uniform compression. However, the effect of ice matrix is not as influential in fine-grained soils. This is because fine-grained soils are already relatively cohesive, thus further increase in ice cohesion does not help increase their bulk moduli. As a result, the association of bulk modulus with total moisture content is not evident in

fine-grained soils.

Fig. 6a-c show the variations of shear modulus with temperature for sand, sand with fines, and fine-grained soils, respectively. Similar to bulk modulus, shear modulus decreases gradually when temperature increases from -30 to -5 $^{\circ}$ C and then decreases rather rapidly when temperature increases from -5 to 0 °C. The shear moduli also quickly reduce to zero after the temperature is above 0 °C. Similar color-coded markers are used in Fig. 6 with blue representing high total moisture contents and vellow presenting low total moisture contents. A red marker is used when the total moisture content is not reported. For sand (Fig. 6a), the markers transition from green to blue (i.e., increased total moisture content) with increasing shear modulus. Nonetheless, there are exceptions for the data reported by Li (2009) in Fig. 6a. Although the data by Li (2009) have higher total moisture contents (30-34%) than those (8-22%) reported by Nakano and Arnold (1973), Li (2009) used fine sand rather than medium sand, resulting in lower shear moduli in Li (2009) even though the soil has higher total moisture content. This shows soil composition is another factor affecting shear modulus. The effect of total moisture content on shear modulus is not evident for sand

Table 2 *P*-values for evaluating the associations between geophysical and geomechanical properties and their influence factors.

Geophysical and Geomechanical Properties	Soil Types	Influence Factors		
		Temperature, T	Total moisture content, w _t	Dry unit weight, γ_d
Bulk modulus, <i>K</i>	Sand	$K \sim \text{Ln}(-T+1),$ P = 0.003. Y.	$K \sim w_{\rm t},$ $P = 0.003. \text{ Y}.$	Not available
	Sand with fines	$K \sim \text{Ln}(-T+1),$ P = 0.000. Y.	$K \sim w_{\rm t}, P = 0.000. { m Y}.$	Not available
	Fine-grained soils	$K \sim \text{Ln}(-T+1),$ P = 0.001. Y.	$K \sim w_{\rm t},$ $P = 0.021. \text{ N}.$	Not available
Shear modulus, G	Sand	$G \sim \text{Ln}(-T+1),$ P = 0.000. Y.	$G \sim w_{t},$ P = 0.080. N.	Not available
	Sand with fines	$G \sim \text{Ln}(-T+1),$ P = 0.000. Y.	$G \sim w_{\rm t},$ P = 0.568. N.	Not available
	Fine-grained soils	$G \sim \text{Ln}(-T+1),$ P = 0.000. Y.	$G \sim w_{\rm b}$ P = 0.778. N.	Not available
	Sand	$\sigma_{ m d} \sim T, \ P=0.398. \ m N.$	Not applicable	Not available
Maximum deviatoric stress, σ_d	Fine-grained soils	$\sigma_{ m d}\sim T, \ P=0.000. \ m Y.$	Not applicable	Not available
	Organic soils	$\sigma_{ m d}\sim T, \ P=0.000. \ m Y.$	Not applicable	Not available
Friction angle, ϕ	Sand	$tan(\phi) \sim T$, $P = 0.742$. N.	$\phi \sim w_{\rm t},$ $P = 0.002. ext{ Y}.$	Not available
	Fine-grained soils	$tan(\phi) \sim T,$ P = 0.578. N.	$\phi \sim w_{\rm t}, \ P=0.042. \ { m N}.$	Not available
Cohesion, c	Sand	$c \sim T$, $P = 0.001$. Y.	$c \sim w_{\rm t},$ P = 0.053. N.	Not available
	Fine-grained soils	$c \sim T$, $P = 0.000$. Y.	$c \sim w_{\rm t},$ P = 0.000. Y.	Not available
Unfrozen water content, w_u	Sand	$Ln(w_u) \sim Ln(-T),$ P = 0.000. Y.	$w_{\rm u}^{1/2} \sim w_{\rm t},$ P = 0.060. N.	Not available
	Sand with fines	$Ln(w_u) \sim Ln(-T),$ P = 0.000. Y.	$w_{\rm u}^{1/2} \sim w_{\rm t},$ P = 0.329. N.	Not available
	Fine-grained soils	$Ln(w_u) \sim Ln(-T),$ P = 0.000. Y.	$w_{\rm u}^{1/2} \sim w_{\rm b}$ P = 0.000. Y.	Not available
Hydraulic conductivity, k_w	Fine-grained soils	$Ln(k_w) \sim Ln(-T+1),$ P = 0.000. Y.	$\operatorname{Ln}(k_w) \sim w_{\mathfrak{b}}$ P = 0.042. N.	Not available
Thermal conductivity, k_h	Sand	$k_h \sim T^2$, P = 0.469. N.	Not available	Not available
	Sand with fines	$k_h \sim T^2,$ P = 0.002. Y.	Not available	Not available
Thermal conductivity, Na	Fine-grained soils	$k_h \sim T^2,$ P = 0.000. Y.	Not available	Not available
	Organic soils	$k_h \sim T^2,$ P = 0.010. N.	Not available	Not available
	Gravel	No effect	Not available	$\varepsilon \sim \text{Ln}(\gamma_d),$ P = 0.000. Y.
	Sand	No effect	Not available	$\varepsilon \sim \text{Ln}(\gamma_d),$ $P = 0.000. \text{ Y}.$
Thaw strain, $arepsilon$	Sand with fines	No effect	Not available	$\varepsilon \sim \text{Ln}(\gamma_d),$ P = 0.000. Y.
	Fine-grained soils	No effect	Not available	$\varepsilon \sim \operatorname{Ln}(\gamma_d),$ $P = 0.000. \text{ Y}.$
	Organic soils	No effect	Not available	$\varepsilon \sim \text{Ln}(\gamma_d),$ P = 0.000. Y.

Note: "Y" means strong associations (P-value <0.005) between a property and its possible influence factors. "N" means weak or no associations (P-value ≥0.005).

with fines (in Fig. 6b) and fine-grained soils (in Fig. 6c). Fig. 6d shows the boxplots of shear moduli for different soil types across various ranges of temperature. Sand overall has higher median shear modulus than sand with fines and fine-grained soils. As shown in the boxplots, the presence of fines greatly reduces the shear moduli. This observation indicates that fines content drives the changes in soil properties. Nonetheless, the difference between the shear moduli of sand with fines and fine-grained soil is not as significant as the difference between sand and sand with fines.

The shear moduli collected in this study were also obtained through ultrasonic tests with frequency mostly ranging from 400 kHz to 2 MHz. Several exceptions include dataset by Meng et al. (2008), which used 50 kHz in the ultrasonic test; this frequency is relatively low when compared to frequencies reported by other references. Meanwhile, Kim et al. (2015) used resonant column, Lee et al. (2002) used hydrostatic compression, and Zhang et al. (2018) used bender element and bending

disk tests to obtain the moduli. This study focuses on identifying the factors that have more significant effects on the moduli such as temperature, soil composition, and soil type. Thus, the deviations in the moduli due to testing methods cannot be captured under this scope and are not further explored.

Regression analyses are undertaken to quantify the variations of shear modulus with temperature and total moisture content. Similar to bulk modulus, shear modulus is also linearly associated with the natural logarithm of temperature for all soil types with *P*-value less than 0.005 (see Table 2). This shows shear modulus is strongly associated with temperature. On the other hand, shear modulus is not strongly associated with total moisture content (*P*-value >0.005) for all soil types. Table 2 also shows that the *P*-value for the relationship between shear modulus and total moisture content increases with fines content. The results indicate that the effect of total moisture content on shear modulus is minimal and such effect diminishes with saline fines content.

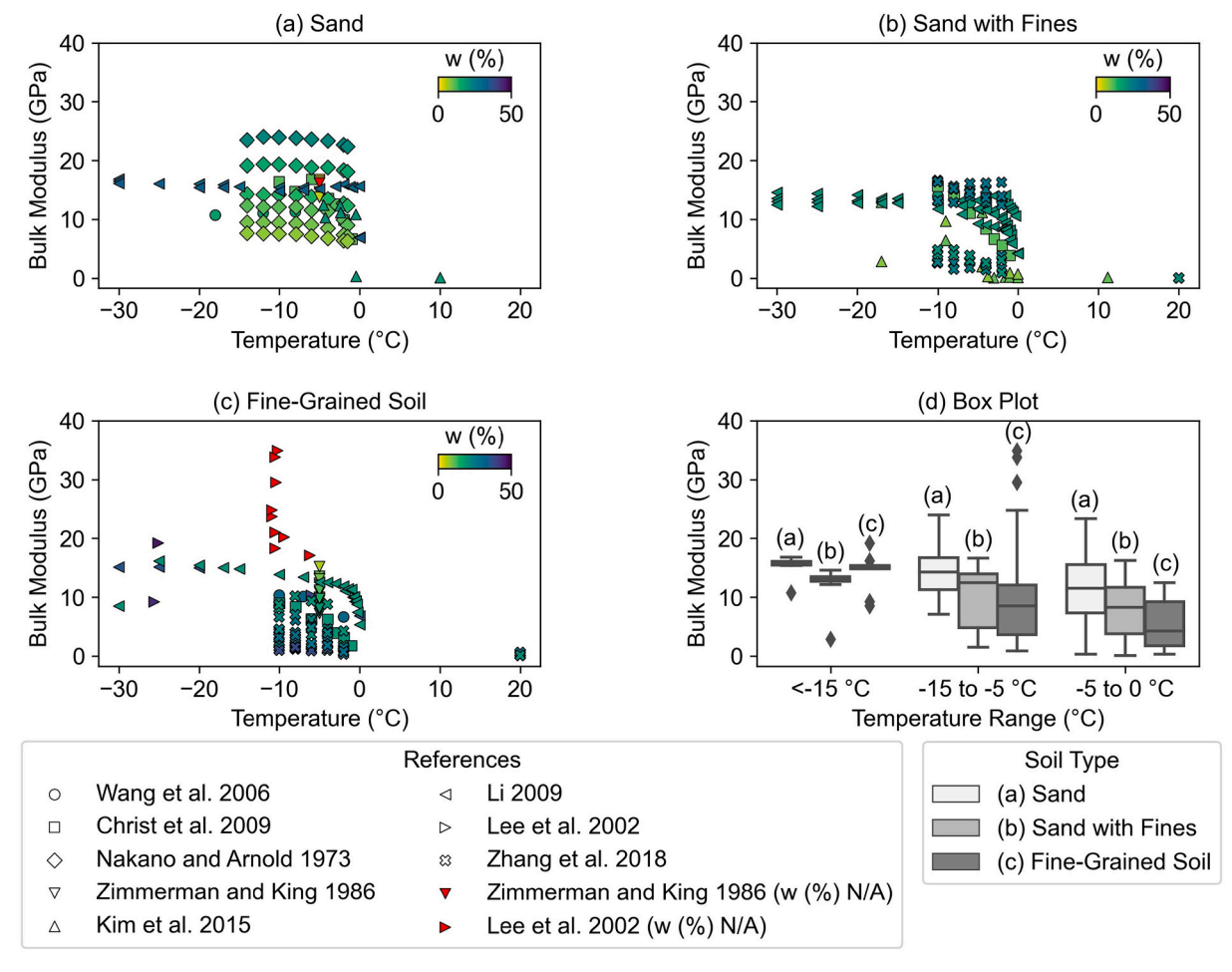


Fig. 5. Variations of bulk modulus with temperature for (a) sand, (b) sand with fines, and (c) fine-grained soils with (d) boxplots comparing bulk moduli for different soil types across different ranges of temperature (Wang et al., 2006; Zimmerman and King, 1986).

The effect of freezing point depression on shear modulus driven by fines content and salinity content is deemed more significant than the effect of overall increase in total moisture content. In other words, for soils with high fines content and salinity content, higher total moisture content does not increase the shear modulus.

7. Reduction of soil strength upon warming

The strength parameters collected in this study were determined using uniaxial compression test, triaxial compression test, and direct shear test. Fig. 7a-c illustrate that the maximum deviatoric stress decreases with increasing temperature despite of the highly scattered data. Based on the regression analysis, maximum deviatoric stress is linearly associated with temperature for all soil types except for sand; its P-value equals to 0.398, greater than 0.005. The P-values are both 0.000 for finegrained soils and organic soils. As depicted in Fig. 7d, sand has a higher average maximum deviatoric stress than fine-grained soils and organic soils at temperatures ranging from −26 to 0 °C. In Fig. 7b, the maximum deviatoric stresses reported by Shelman et al. (2014) range from 3500 to 13,500 kPa. The variation of the dry unit weights $(8-30 \text{ kN/m}^3)$ of these specimens is responsible for such significant variation of the stresses under the same temperature (–20 $^{\circ}\text{C}$). The collected data suggest that maximum deviatoric stress increases with increasing dry unit weight. The total moisture content is not reported in Ma et al. (1993) in Fig. 7a; this likely causes the data scatter.

The color-coded markers in Fig. 7 represent the confining pressure at which the maximum deviatoric stress is measured. The collected data suggest that maximum deviatoric stress is independent of confining

pressure (in the range of 0-20 MPa). This conclusion is supported by some references. Arenson and Springman (2005) reported that deviatoric shear strength, including peak and residual strengths, is independent of confining stress (0-450 kPa). However, some studies show contrasting results. Parameswaran and Jones (1981) and Ting et al. (1983) reported that maximum deviatoric stress and shear strength increase with increasing confining stress (0-40 MPa). These additional data are not plotted in Fig. 7 because the exact temperature for each datapoint was not reported. Based on these findings, we reason that maximum deviatoric stress is only weakly associated with a narrow range of confining stress. Especially in the range of confining stress concerned by geotechnical engineers, the effect of confining stress on frozen soils is not as influential as the effects of other factors (e.g., temperature, soil type). The boxplots in Fig. 7d show that the presence of fines content greatly reduces the maximum deviatoric stress across different ranges of temperature. Fig. 7d also shows the maximum deviatoric stresses of organic soil are comparable to those of fine-grained soils in temperature ranges of -15 °C < T < -5 °C and -5 < T < 0 °C.

Shear strength parameters of friction angle and effective cohesion collected from literature are presented in Figs. 8 and 9, respectively. The regression analysis of the collected data suggests that the tangent of friction angle does not correlate with temperature (the P-values are higher than 0.005 for both sand and fines) whereas cohesion is linearly associated with temperature (the P-values for sand and fines are less 0.005). For friction angle, the high P-values based on the collected data suggest that temperature does not cause the variation of friction angle. For example, in Fig. 8, the variation of the effective friction angles under the same temperature ($-6.5\,^{\circ}$ C) in Tong (1983) is due to the variation of

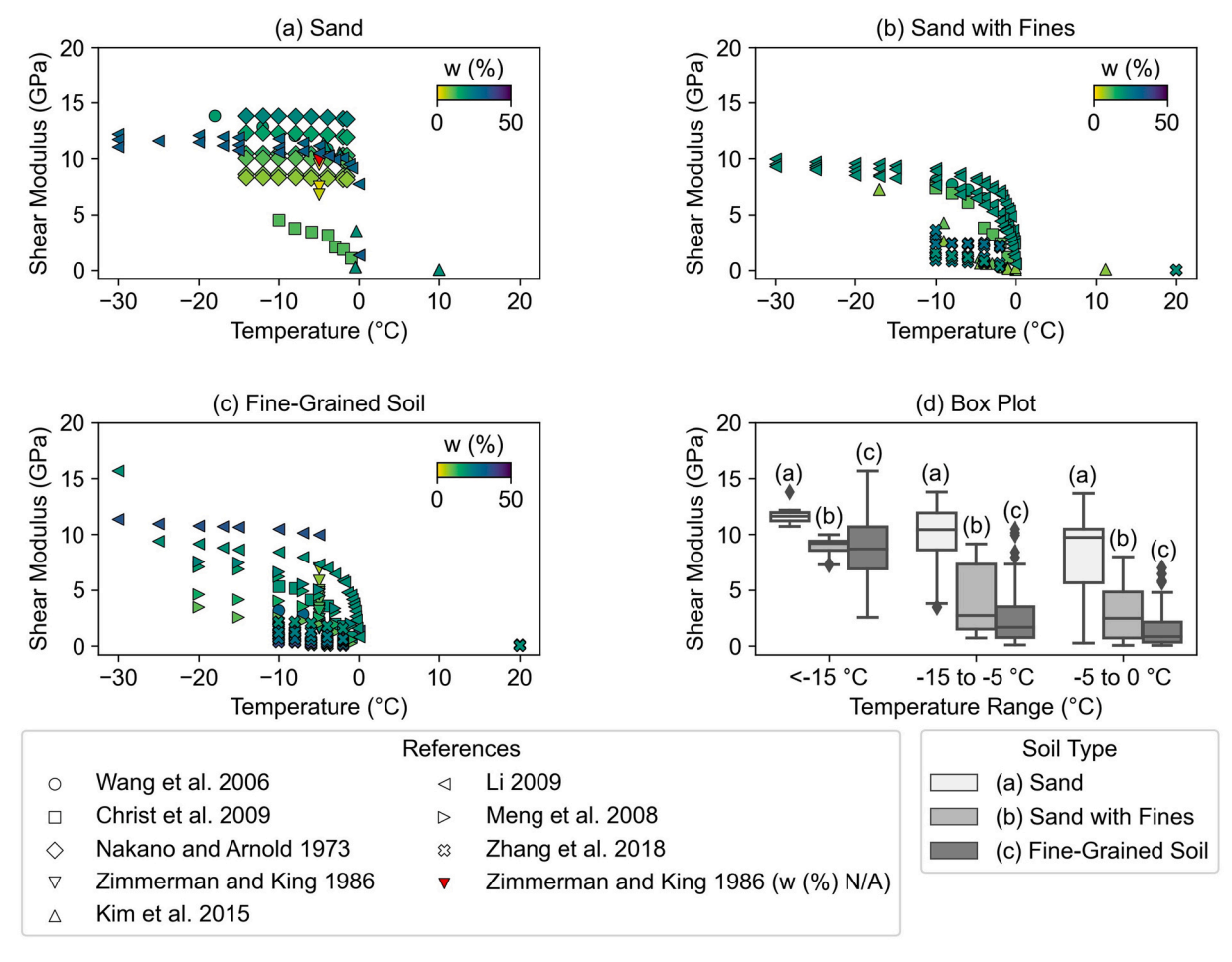


Fig. 6. Variations of shear modulus with temperature for (a) sand, (b) sand with fines, and (c) fine-grained soils with (d) boxplots comparing shear moduli for different soil types across different ranges of temperature.

the confining pressure (20–207 kPa), while the data variation in Hanna and McRoberts (1988) is due to the variation of total moisture content (25–30%). For cohesion, the low *P*-values suggest that temperature controls the cohesion.

Regression analysis was also performed to evaluate the influence of total moisture content on friction angle and cohesion. As summarized in Table 2, for sand, friction angle is associated with total moisture content (P-value = 0.002), but cohesion is not (P-value = 0.053). For finegrained soils, friction angle is not associated with total moisture content (P-value = 0.042), but cohesion is associated with total moisture content (P-value = 0.000). This observation can be explained as following. Shear strength of sandy soils is mostly contributed by the friction, whereas shear strength of fine-grained soils is contributed mainly by cohesion. As total moisture content increases, ice matrices increase the distance between soil grains and reduce the effects of their friction or cohesion. As a result, an increase in total moisture content only influences the major shear strength parameter of a soil. Since friction angle is the major shear strength parameter for sandy soils, total moisture content is strongly associated with friction angle but not cohesion in sand. Conversely, total moisture content is strongly associated with cohesion but not friction angle in fine-grained soils.

8. Increased unfrozen water content and hydraulic conductivity upon warming

The unfrozen water content highly depends on soil temperature and soil type (Christ et al., 2009; Li et al., 2020; Tang et al., 2020). Some relationships between unfrozen water content and negative soil

temperature have been established in the literature as presented in Eqs. (5) and (6).

$$w_u = w_0 + A \left(\frac{1}{1 + \alpha |T - T_f| + \beta (T - T_f)^2} - 1 \right)$$
 (5)

$$w_u = \alpha |T|^{\beta} \tag{6}$$

where w_u is the gravimetric unfrozen water content in percentage, w_0 is the gravimetric unfrozen water content at T_f , T_f is the freezing point of water, which is 0 °C, T is the negative soil temperature in °C, and A, α and β are soil-type dependent parameters. Given the simplicity of Eq. (6), it is used in the regression analysis to evaluate the effects of temperature on the gravimetric unfrozen water content for various soil types. Fig. 10a-c present the data for sand, sand with fines, and finegrained soils, respectively. All three sub-figures show that unfrozen water content increases with increasing temperature for all soil types. However, it is important to note that the y-axes are on different scales: sand and sand with fines have a lower range of unfrozen water contents $(10^{-2}-10^{2}\%)$ and fine-grained soils with a higher range $(10^{-2}-10^{3}\%)$. The regression analyses show that the natural logarithm of unfrozen water content is linearly associated with the natural logarithm of temperature; the P-values are 0.000 for all soil types. Boxplots comparing the gravimetric unfrozen water contents of different soil types for various temperature ranges are presented in Fig. 10d. This sub-figure shows that fine-grained soils have higher median unfrozen water content than sand with fines and sand across the three ranges of temperature. Fine-grained soils also have wider range and interquartile range of

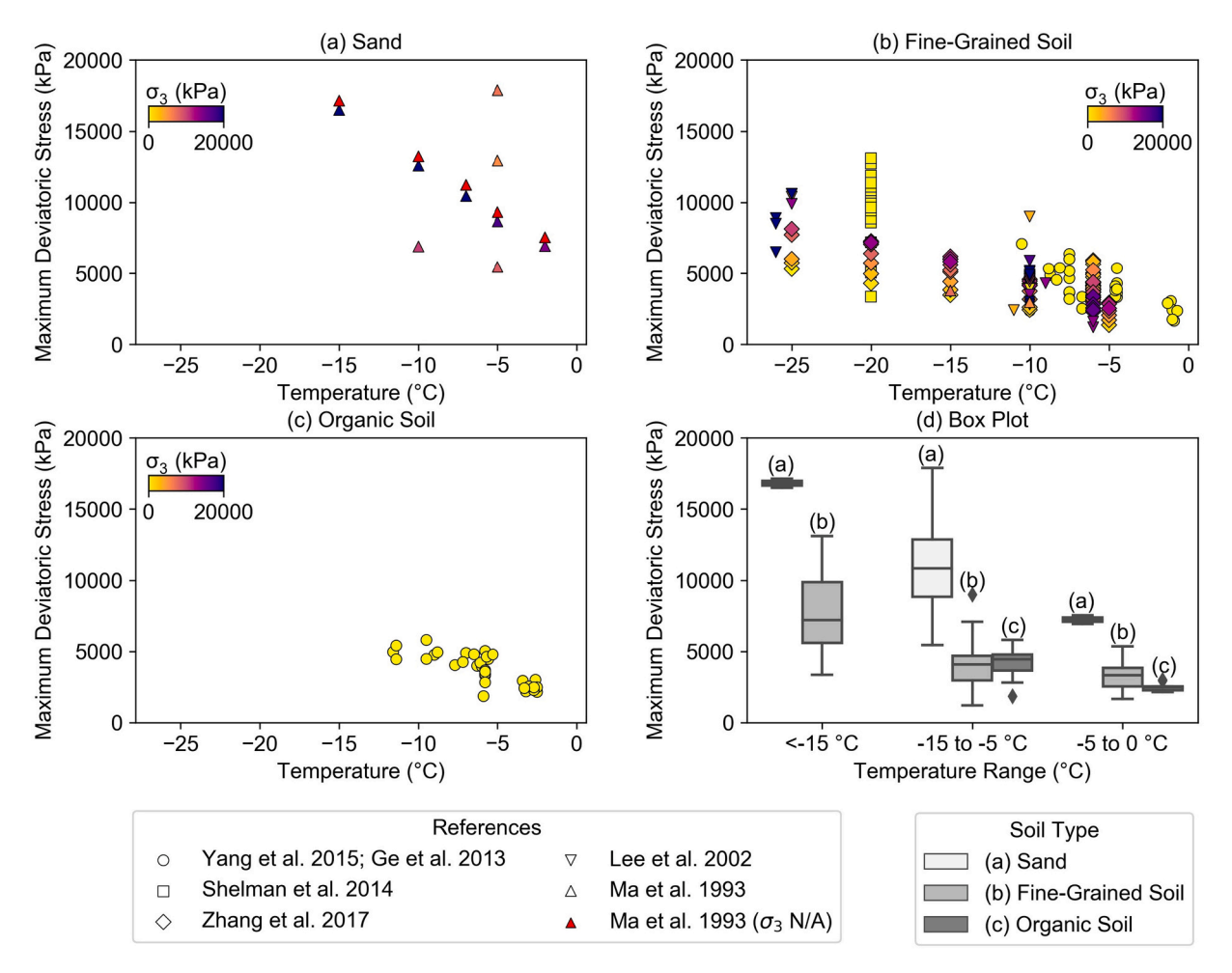


Fig. 7. Variations of maximum deviatoric stress with temperature for (a) sand, (b) fine-grained soils, and (c) organic soils with (d) boxplots comparing maximum deviatoric stresses for different soil types across different ranges of temperature (Yang et al., 2015; Zhang et al., 2017).

gravimetric unfrozen water content across the three different temperature ranges.

Regression analysis is also conducted to evaluate the influence of total moisture content on the gravimetric unfrozen water content. The regression analysis, which is summarized in Table 2, shows that the square root of gravimetric unfrozen water content is associated with the total moisture content only for fine-grained soils (P-value = 0.000) but not for sand (P-value = 0.060) and sand with fines (P-value = 0.329). This finding is also reflected by the color-coded markers in Fig. 10a-c. In Fig. 10c, the markers gradually transition from yellow to blue as gravimetric unfrozen water content increases. There is an exception: datapoints by Christ et al. (2009) have relatively low gravimetric unfrozen water content despite higher total moisture content. We suspect that testing methods may be responsible for such discrepancy. The data by Christ et al. (2009) were determined using time domain reflectometry (TDR). The determination of unfrozen water content using TDR requires precise calibration of the relationship between apparent dialectic constant and water content; however, the dielectric constant for adsorbed water is slightly lower than that of free water (Smith and Tice, 1988). Since fine-grained soil has a higher specific surface area (SSA) than sand and sand with fines, more water is adsorbed in fine-grained soil. As a result, the unfrozen water content determined using TDR is lower than the value determined using nuclear magnetic resonance (NMR) for soil samples with high SSA (Smith and Tice, 1988). It is worth noticing that NMR was used in all references, except for Christ et al. (2009) (using TDR), Li (2009) (using frequency domain reflectometry), and Fu et al. (1983) (using ultrasonic).

The findings in Section 8 (unfrozen water content) are correlated to those in Section 6 (elastic modulus) and 7 (soil strength). The reduction of soil modulus and strength upon warming is due to the increase of unfrozen water content as soil temperature increases as presented in Fig. 10. Given a constant moisture content, an increase in unfrozen water content also means a reduction in ice content. Several authors pointed out that unconfined compressive strength, yield strength, and shear wave velocity decrease with a decrease in ice content; such trends are more obvious at higher temperatures (> -6 °C) (Yang et al., 2012; Ge et al., 2012, 2013). Other studies also reported similar findings: strength increases with an increasing degree of ice-saturation (Ting et al., 1983) or increasing ice content (Jessberger, 1980) provided that the relative density of the soil skeleton remains the same. For coarsegrained soils, shear strength can be defined as a function of volumetric ice content (Arenson and Springman, 2005). As ice content increases, suction also increases, resulting in higher effective stress and therefore higher ultimate shear strength (Arenson et al., 2007). There also exist two different ice-forming mechanisms that cause fine-grained soils to have lower strength (Figs. 7-9) and elastic moduli (Figs. 5-6). For coarse-grained soils, the soil skeleton usually cools down before the unfrozen water. Consequently, unfrozen water is located in the middle of the pore space (Arenson and Sego, 2006). For fine-grained soils, unfrozen water forms a film that surrounds soil particles and ice forms in the middle of the pore space (Arenson and Sego, 2006). These different ice structures can influence the strength of frozen soil.

Salt content can also influence the geomechanical properties by increasing the unfrozen water content of frozen soil at any given

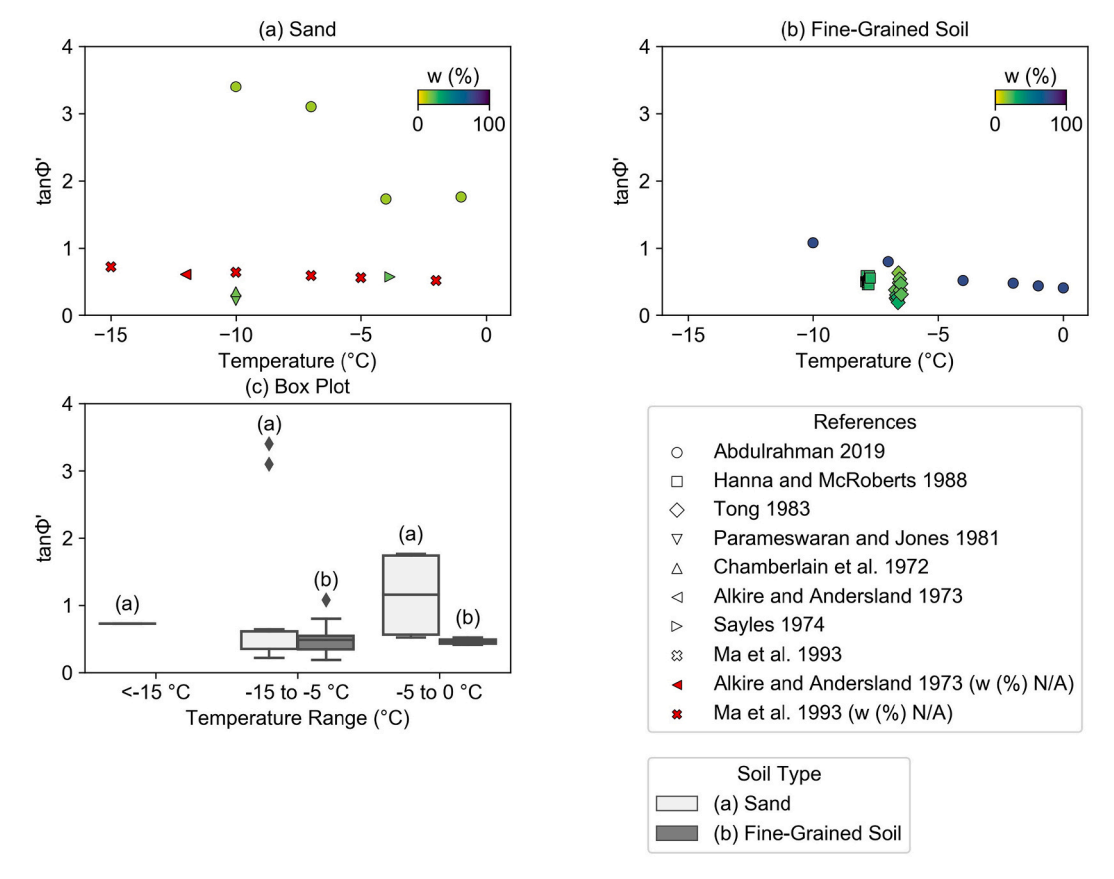


Fig. 8. Variations of the tangent of effective friction angle with temperature for (a) sand and (b) fine-grained soils with (c) boxplots comparing the tangent of effective friction angle for different soil types across different ranges of temperature (Abdulrahman, 2019; Chamberlain et al., 1972; Alkire and Andersland, 1973; Sayles, 1974).

temperature. This characteristic is responsible for part of the data scatter in Fig. 10. The increase in unfrozen water content due to salinity is captured by Arenson and Sego (2006). In warmer non-saline soils, ice exists as an ice matrix encompassing soil grains with pockets of unfrozen water (Arenson and Sego, 2006). However, ice in colder saline soils exists in the form of ice needles, which are surrounded by channels of unfrozen water. Given that needle-shaped ice has lower strength than ice in matrix form, a cold saline soil has a lower strength than a warm non-saline soil with an equivalent amount of unfrozen water (Arenson and Sego, 2006).

Hydraulic conductivity is one of the important parameters in understanding permafrost degradation since it controls the flow of water to the freezing front. Hydraulic conductivity data collected in this study were determined using dilatometer. The collected data suggest that hydraulic conductivity increases with increasing temperature as presented in Fig. 11. Based on the regression analysis as presented in Table 2, the natural logarithm of hydraulic conductivity is linearly associated with the natural logarithm of temperature with a P-value of 0.000. This is because unfrozen water content increases with increasing temperature. This increases the number of pathways of water flow. Hydraulic conductivity, however, is not associated with the total moisture content of soil specimens (P-value = 0.042). This observation can be explained as follows. In unfrozen soil, hydraulic conductivity often increases with an increase in total moisture content. This is because the porosity increases as the total moisture content per unit volume of soil grains increases, allowing more water to flow through the soil. However, in frozen soils, the increase in total moisture content does not contribute to the increase of hydraulic conductivity because the moisture is mostly in its solid form (i.e., ice), which impedes the flow of water.

9. Variations of thermal conductivity and heat capacity upon warming

Thermal conductivity data collected in this study were obtained using conductivity copper probe in Riseborough et al. (1983) and stationary thermal regime method in Barkovskaya et al. (1983). Fig. 12a-d show the variations of thermal conductivity with temperature for sand, sand with fines, fine-grained soils, and organic soils, respectively. The data still appear relatively scattered despite being categorized into different groups of soil types (i.e., sand, sand with fines, fine-grained soils, and organic soils). In general, thermal conductivity increases to a maximum value as temperature decreases but then slightly decreases as temperature continues to decrease. This general trend is explained as follows. The thermal conductivity of ice is 2.21 W/m.°C at 0 °C and 2.66 W/m⋅°C at −40 °C, and the thermal conductivity of water is 0.56 W/ m.°C at 0 °C and 0.58 W/m.°C at 10 °C (Andersland and Ladanyi, 2004). This indicates that thermal conductivity increases with decreasing unfrozen water content. Therefore, as temperature decreases, unfrozen water content decreases, thus thermal conductivity increases. The increase in thermal conductivity is more apparent at around 0 °C given the more drastic decrease in the unfrozen water content at that temperature. As temperature further decreases (starting around -2 to -5 °C), the thermal conductivity slightly reduces. This reduction is due to the microcracks in ice (i.e., ice fragmentation owing to the thermomechanical stresses) (Barkovskaya et al., 1983).

In addition to temperature, thermal conductivity is also affected by salinity as depicted in Fig. 12a. At any given temperature, as salinity increases, unfrozen water content increases. As a result, thermal conductivity decreases. Comparing the data across different soil types, sand (without fines or salt content) typically has the highest thermal conductivity; the maximum value measured is approximately 2.5-3.0~W/

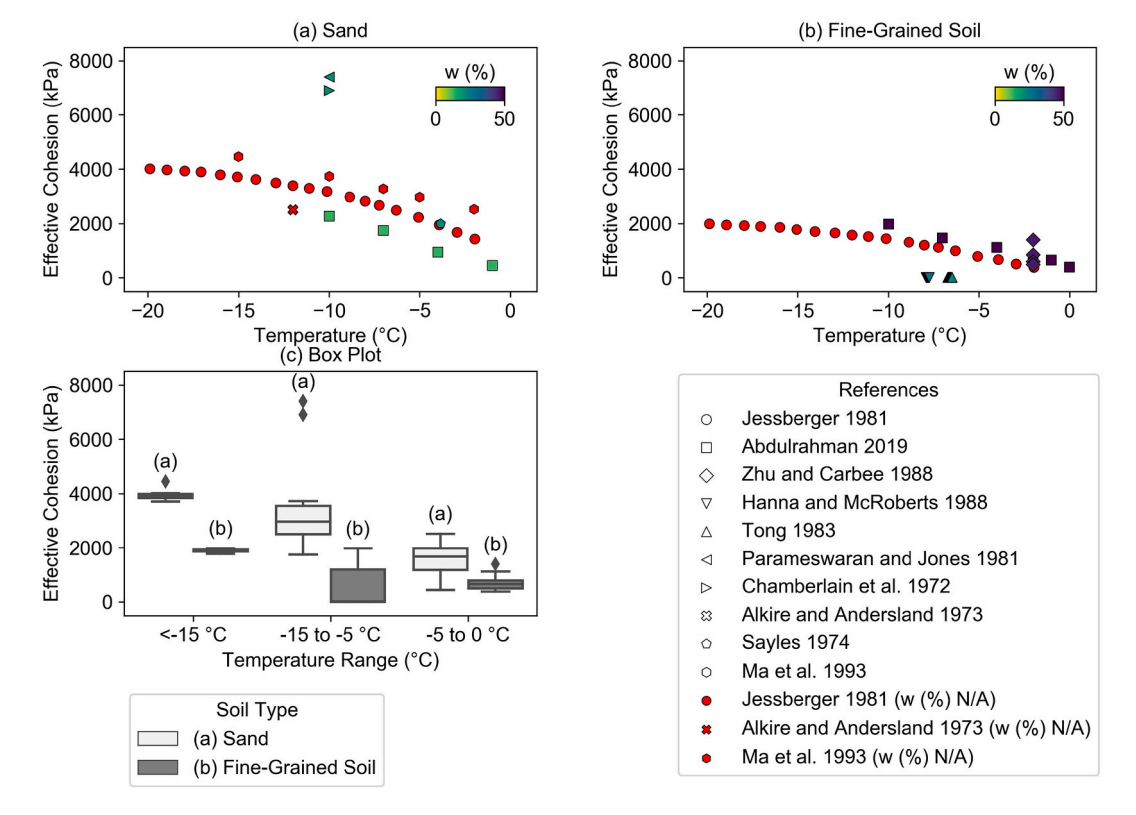


Fig. 9. Variations of effective cohesion with temperature for (a) sand and (b) fine-grained soils with (c) boxplots comparing the effective cohesion for different soil types across different ranges of temperature (Zhu and Carbee, 1988; Gregersen et al., 1983; McGaw et al., 1983; Oliphant et al., 1983; Aksenov et al., 1998; Furuberg and Berggren, 1988).

 $m\cdot^{\circ}C$. Fine-grained soils and organic soils have lower thermal conductivities (1.5 W/ $m\cdot^{\circ}C$ and 2.0 W/ $m\cdot^{\circ}C$, respectively). So, peat or fines contents, if present in a soil specimen, can reduce the overall thermal conductivity of the soil (see Fig. 12b). Thermal conductivity of fine-grained soils is also affected by the types of clay mineral (e.g., montmorillonite, kaolinite) as shown in Fig. 12c.

Regression analysis is performed to evaluate the association between thermal conductivity and temperature. As presented in Table 2, the thermal conductivities of sand with fines and fine-grained soil are strongly associated with the quadratic function of temperature with *P*-values of less than 0.005. Based on the currently available data, it is suggested that the same relationship also exists for organic soils given their relatively low *P*-value (0.010). Nevertheless, the data collected in this study suggest that the thermal conductivity of sand does not correlate with temperature with a *P*-value of 0.469, significantly greater than 0.005. This is because the sand data in Fig. 12a are greatly affected by salinity. Consequently, the influence of temperature, which is relatively weak in this case, cannot be captured.

In references on numerical models (Thomas et al., 2009; Yamamoto, 2013; Zhang and Michalowski, 2015), thermal conductivity of the soil matrix is expressed in various forms:

$$k_{h_{-m}} = k_{h_{-i}}^{\theta_i} \cdot \mathbf{k}_{h_{-w}}^{\theta_w} \cdot \mathbf{k}_{h_{-s}}^{\theta_s} \tag{7}$$

or,

$$k_{h_m} = k_{h_w}\theta_w + k_{h_i}\theta_i + k_{h_s}\theta_s \tag{8}$$

where $k_{\rm h}$ is thermal conductivity; θ is the volumetric fraction of soil constituent. The subscripts m, w, i, and s refer to soil matrix, water, ice, and soil grains, respectively. It is noted that the thermal conductivity expressed in these forms rely on the accurate prediction of the amount of unfrozen water content. In Fig. 10, as temperature decreases, the amount of unfrozen water content decreases to zero, and the amount of

ice content approaches the total moisture content. Based on Eqs. (7) and (8), the thermal conductivity of the soil specimens would have been the same once all unfrozen water changes phase to ice. However, Fig. 12 shows a slight reduction of thermal conductivity at lower temperatures. So, there exists a slight discrepancy between the experimental data and the theoretical prediction using Eqs. (7) and (8). The effects of such discrepancies on numerical model results need to be evaluated in future research.

The currently available data suggest that heat capacity increases with increasing temperature as shown in Fig. 13. The regression analysis shows that the natural logarithm of heat capacity is linearly associated with the natural logarithm of temperature with a *P*-value of 0.000. The increase in unfrozen water content due to temperature increase (as depicted in Fig. 10) is likely to be responsible for the increase in heat capacity in Fig. 13 (Hansson et al., 2004).

In most references on numerical modeling of seasonally frozen soils and permafrost for engineering purposes (Roth and Boike, 2001; Thomas et al., 2009; Yamamoto, 2013; Zhang and Michalowski, 2015), volumetric heat capacity of soil mixture is defined as

$$c_h = \rho_w c_{h-w} \theta_w + \rho_i c_{h-i} \theta_i + \rho_s c_{h-s} \theta_s \tag{9}$$

where $\rho=$ density, $c_h=$ mass heat capacities, $\theta=$ volumetric fraction, and the subscripts w, i, and s refer to water, ice, and soil grains, respectively. References (Anisimov et al., 1997; Liu et al., 2021), which consider permafrost degradation at the hemispheric scale, focused on only two states of volumetric heat capacity (i.e., frozen or thawed). The frozen volumetric heat capacity, $c_{h,frozen}$, and thawed volumetric heat capacity, $c_{h,thawed}$ are defined as

$$c_{h-frozen} = c_s \rho_s + 2025 w \tag{10a}$$

$$c_{h_thawed} = c_s \rho_s + 4190 w \tag{10b}$$

where c_s is the dry soil's heat capacity, and w is relative soil moisture

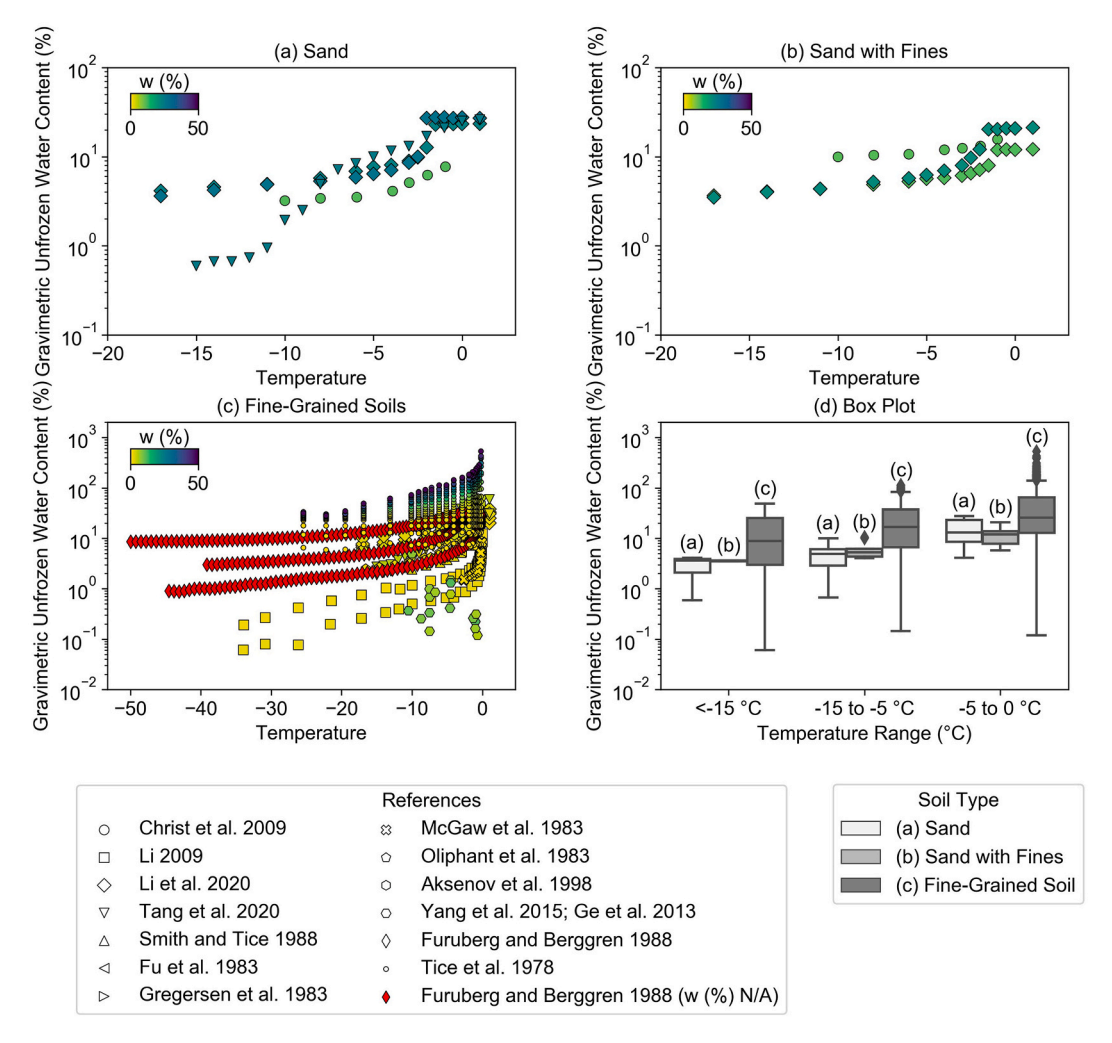


Fig. 10. Variations of gravimetric unfrozen water content with temperature for (a) sand, (b) sand with fines, and (c) fine-grained soils with (d) boxplots comparing the gravimetric unfrozen water content for different soil types across different ranges of temperature.

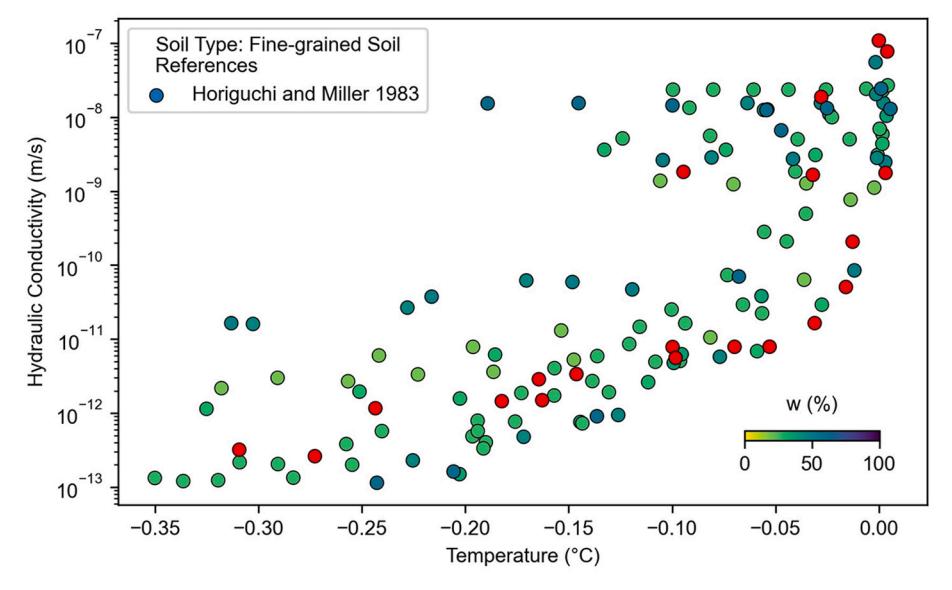


Fig. 11. Variations of hydraulic conductivity with temperature.

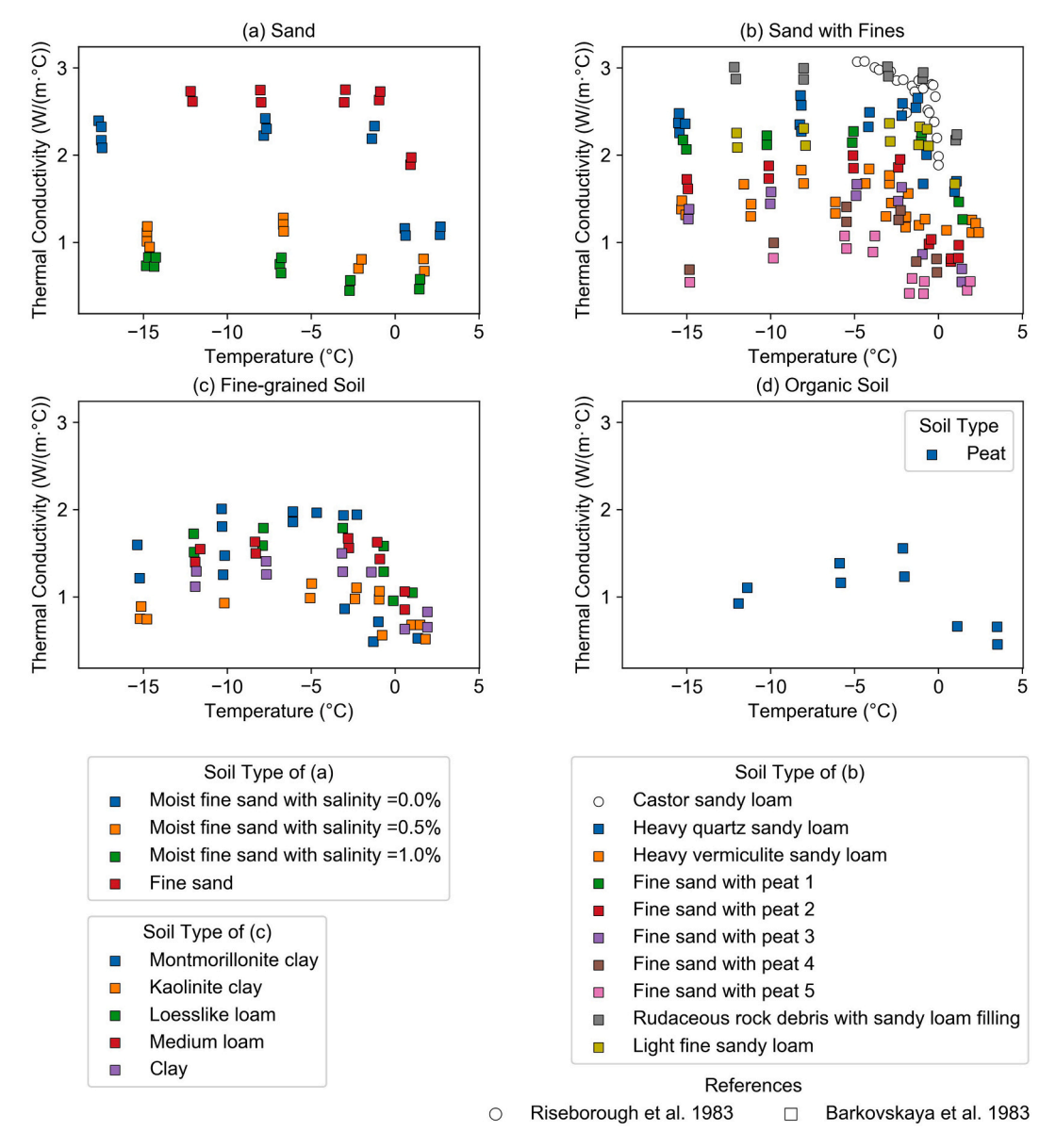


Fig. 12. Variations of thermal conductivity with temperature for (a) sand, (b) sand with fines, (c) fine-grained soils, and (d) organic soils.

content.

Time periods being considered for a civil engineering application are typically shorter than those for geosciences, demanding predictions with shorter time frame but higher temporal resolution. It is necessary to use a more accurate volumetric heat capacity in infrastructure-related problems. The volumetric heat capacity can be improved by using either Eq. (9) (which relies on the accuracy of the amount of unfrozen water in the soil), or directly validated using experimental data of volumetric heat capacity such as those in Fig. 13.

10. Thaw strain

The collected data in Fig. 14 show that thaw strain is higher for soil with lower dry unit weight. Based on the regression analyses, thaw strain is linearly proportional to natural logarithm of dry unit weight for all soil types, and the P-values are 0.000. The equations for predicting thaw strains for various soil types (gravel, sand with fines, and finegrained soils) are presented in Eqs. (11)–(13) with R^2 values ranging from 74.3% to 79.1%. Regression equations for sand and organic soils, however, are not presented due to the high variability (i.e., low R^2) in

the data. As depicted in Fig. 14, soils that experience excessive thaw strain (ε >50%) are mostly organic soils and fine-grained soils. Boxplots comparing the thaw strain for different types of soil are presented in Fig. 15. Since thaw strain depends significantly on the dry unit weight of soil, the ranges of thaw strain are wide for most of the soil types, especially for fine-grained soils and organic soils due to their high waterabsorbing capability. The boxplots also show that the median thaw strains for fine-grained soils and organic soils are higher than those for gravel, sand, and sand with fines.

Gravel:
$$\varepsilon = 97.8 - 31.5 \ln(\gamma_d)$$
; $R^2 = 77.9\%$; $P - \text{value} = 0.000$ (11)

Sand with fines :
$$\varepsilon = 115.1 - 39.0 \ln(\gamma_d); R^2 = 74.3\%; P$$
 - value = 0.000 (12)

Fines:
$$\varepsilon = 104.4 - 35.9 \ln(\gamma_d)$$
; $R^2 = 79.1\%$; $P - \text{value} = 0.000$ (13)

where ε is thaw strain in %, and γ_d is dry unit weight in kN/m³. Prediction of thaw strain based on density is commonly used in the literature. Crowther (1992) and Pullman et al. (2007) expressed thaw strain, ε , as a function of frozen dry density, $\gamma_{\rm f}$, and settled dry density,

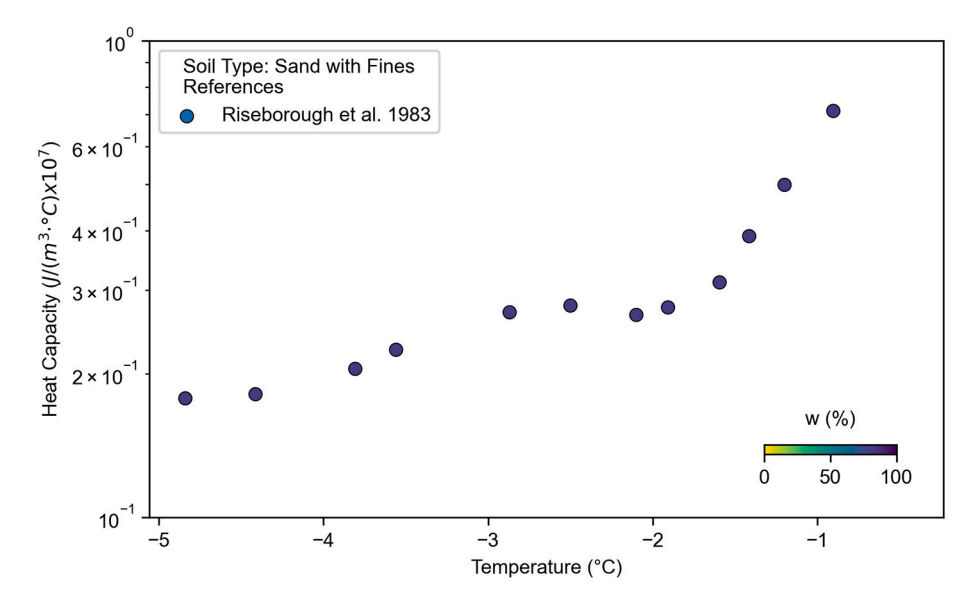


Fig. 13. Variations of heat capacity with temperature.

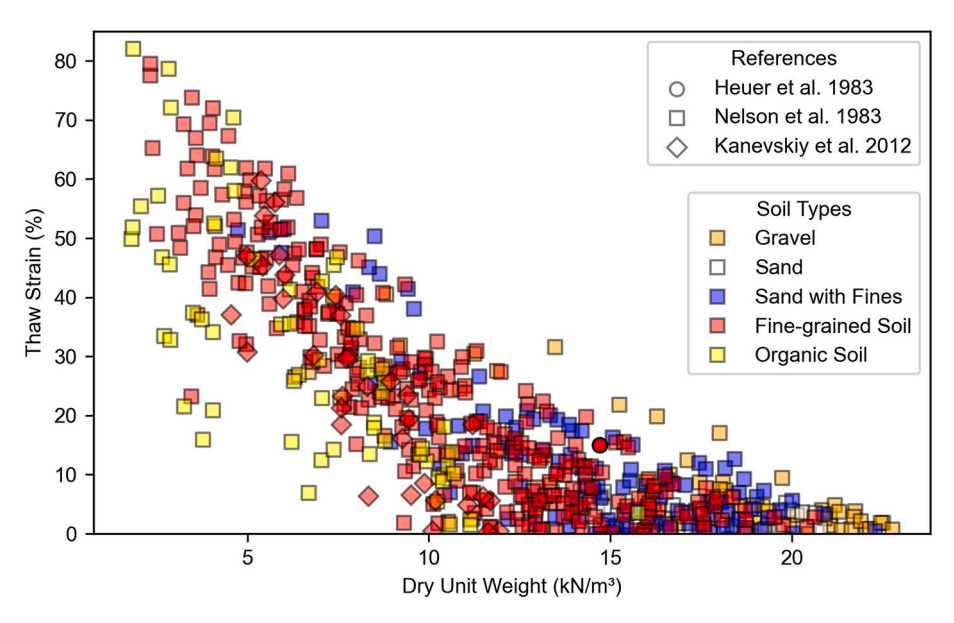


Fig. 14. Variations of thaw strain with dry unit weight (Heuer et al., 1983; Kanevskiy et al., 2012).

$$\gamma_s$$
:
$$\varepsilon = \frac{\gamma_s - \gamma_d}{\gamma_s} \tag{14}$$

Although these equations (Eqs. (11)–(14)) cannot be used to accurately estimate the time-dependent thaw strain during warming of permafrost or seasonally frozen soils under negative temperatures, they provide rough estimations of thaw strain upon thawing of permafrost. These rough estimations of thaw strain can later be used to validate the results of numerical models for different soil types and will be useful for predicting thaw strains for civil infrastructure at a regional scale.

In this study, thaw strain for each soil type is predicted using only dry unit weight (as shown in Eqs. (11)–(13)). On the other hand, Nelson et al. (1983) expressed thaw strain as a function of porosity, n, moisture content, w, and degree of saturation, S:

$$\varepsilon = a n^2 + b n + c \frac{n^2 w}{S} + d \frac{n}{S} + e \frac{n}{w} + f$$
 (15)

where a, b, c, d, e, and f are soil-type dependent coefficients. The R^2 values for gravel, sand with fines, and fines range from 82% to 95% (using Eq. (15) by Nelson et al., 1983) as compared to the R^2 values (i.e., 74% to 79%), which are determined using only dry unit weight (using Eqs. (11)–(13)). The R^2 values increase only by about 10% even after considering two additional parameters and four additional statistical coefficients. However, Eq. (15) may be necessary for sand and organic soil, for which the thaw strain cannot be precisely predicted using only dry unit weight. For sand, R^2 increases from 39% to 83% when using Eq. (15). For organic soil, R^2 increases from 55% to 77%.

11. Knowledge gaps

Based on the data collected in this study, we summarize the knowledge and data that are needed for creating a comprehensive and complete picture of how the geophysical and geomechanical properties of permafrost-affected soil are affected by permafrost degradation. These knowledge gaps include the following:

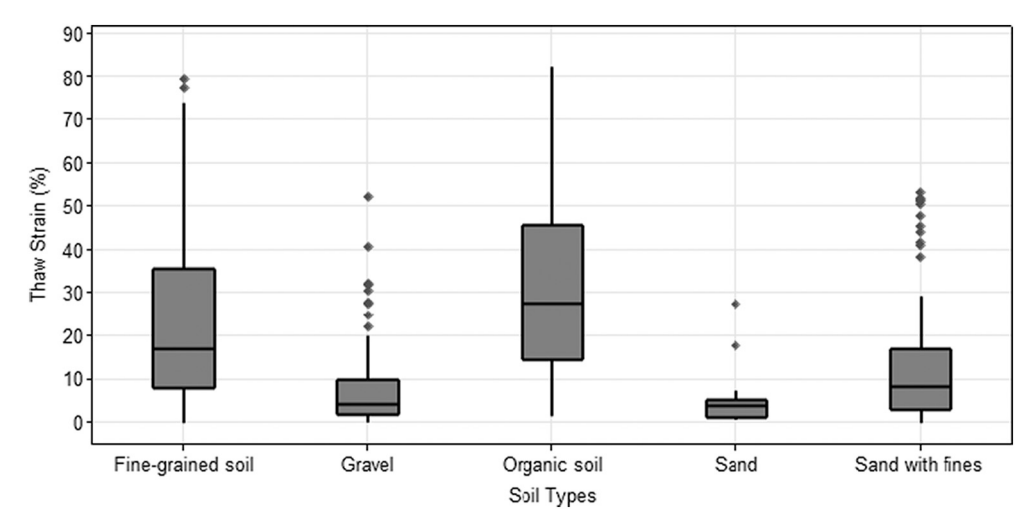


Fig. 15. Boxplots of thaw strain for different soil types.

Table 3Knowledge gaps and the corresponding potential solutions.

Challenges	Proposed solutions
Lack of data from in-situ or representative soil samples Lack of long-term in-situ data	Conduct traditional drilling and laboratory testing Deploy long-term in-situ permafrost
	monitoring stations (Romanovsky et al., 2010)
Variability of in-situ permafrost	Employ statistical approach to account
properties due to heterogeneity of subsoil condition	for and quantify the uncertainty of measurements
Inherent laboratory or in-situ testing errors	As above
Incomplete and nonsystematic database	Build a comprehensive and searchable database of the permafrost properties and develop statistical analysis to identify primary properties when input data (such as soil types and compositions) are provided by users
Complex interrelationships between factors and their effects on the primary properties	Apply machine learning algorithms to distinguish the primary and secondary factors affecting the degree of permafrost degradation (Pierce et al., 2021)

- Elastic moduli for organic soil,
- Stress-strain relationships for sand with fines under compression testing,
- Stress-strain relationships for all soil types under tensile testing,
- Shear strength parameters for sand with fines and organic soil,
- Unfrozen water content for organic soil,
- Hydraulic conductivity for sand, sand with fines, and organic soil,
- · Heat capacity for all soil types.

At present, we are only able to quantify the individual effects of temperature and other factors (e.g., soil types, soil compositions, confining stress) on the geophysical and geomechanical properties. The complete quantifications of their collective effects are still a challenge. To overcome this challenge, Table 3 summarizes the knowledge gaps and lists the potential solutions for each. These challenges must be addressed to ultimately develop a systematic approach to predict the impacts of permafrost degradation on civil infrastructure and quantify the costs needed to maintain civil infrastructures in northern high-latitude regions.

12. Conclusions

This study quantifies the variations of geomechanical and geophysical characteristics of permafrost-affected soils with temperature and explains how other factors contribute to the variations. Based on the collected data, as temperature increases, soil strength and elastic moduli reduce; this results in reduced bearing capacity and increased compressibility. This study also shows that unfrozen water content increases with increasing soil temperature, contributing to higher hydraulic conductivity and water flow. The increase in unfrozen water content is also the primary reason for reduced soil strength during permafrost degradation. Upon warming near 0 °C, the thermal conductivity decreases, and the volumetric heat capacity increases; more energy is needed to increase the temperature of frozen soil at temperatures near the melting point of water. The variations of geomechanical and thermal properties with temperature suggest that permafrost experiences rapid strength degradation at relatively slow temperature increment near the melting point of water.

The regression analyses show that all geomechanical and geophysical properties collected in this study, except for tangent of friction angle, have strong correlations with temperature although the data are highly scattered. In addition to temperature, total moisture content also affects the geomechanical and geophysical properties. The influence of total moisture content on each property also varies significantly for different soil types. Other factors such as grain size, relative density, salinity, and ice-forming mechanisms also affect how the properties vary with temperature and are likely to be responsible for the data scatter. The interrelationships of these factors and their effects on the primary properties are discussed.

Given the limited quantitative data for permafrost-affected soils, it is challenging to quantify and discern the individual and collective effects of these factors. The challenges identified include lack of field and long-term data on permafrost-affected soils and inadequate understanding of the complex interrelationships among various highly varied soil properties, compositions of permafrost-affected soils, and environmental forcing factors. Solutions are proposed accordingly to understand the complex geotechnical mechanisms of permafrost degradation and to facilitate future permafrost model development.

Data availability statement

The data that support the findings of this study are available upon reasonable request from the authors.

CRediT authorship contribution statement

Min Liew: Conceptualization, Methodology, Formal analysis, Investigation, Data curation, Visualization. Xiaohang Ji: Formal analysis, Investigation, Data curation, Visualization. Ming Xiao: Conceptualization, Supervision. Louise Farquharson: Writing – review & editing. Dmitry Nicolsky: Writing – review & editing. Vladimir Romanovsky: Writing – review & editing. Matthew Bray: Writing – review & editing. Xiong Zhang: Writing – review & editing. Christopher McComb: Writing – review & editing.

Declaration of Competing Interest

None.

Acknowledgements

This study was supported by the National Science Foundation under Grant Nos. ICER-1927718, ICER-1927708, ICER-1927715, and CMMI-2034363. The first author was partially supported by the Mark E. and Claire L. Alpert Graduate Fellowship in the Department of Civil and Environmental Engineering at the Pennsylvania State University.

Appendix A. Supplementary data

Supplementary data to this article can be found online at https://doi.org/10.1016/j.coldregions.2022.103522.

References

- Abdulrahman, A.A.H., 2019. Load Transfer and Creep Behavior of Pile Foundations in Frozen Soils. PhD Dissertation. Carleton University, Ottawa, Ontario. https://doi. org/10.22215/etd/2019-13781.
- Aksenov, V.I., Klinova, G.I., Scheikin, I.V., 1998. Material composition and strength characteristics of saline frozen soils. In: Seventh International Conference on Permafrost, Yellow Knife, Canada, 55, pp. 1–4.
- Alkire, B.D., Andersland, O.B., 1973. The effect of confining pressure on the mechanical properties of sand-ice materials. J. Glaciol. 12 (66), 469–481. https://doi.org/ 10.3189/S0022143000031889.
- Allard, M., Lemay, M., Barrette, C., L'Hérault, E., Sarrazin, D., Bell, T., Doré, G., 2012. Permafrost and climate change in Nunavik and Nunatsiavut: Importance for municipal and transportation infrastructures. In: Nunavik and Nunatsiavut: From science to policy. An Integrated Regional Impact Study (IRIS) of Climate Change and Modernization, pp. 171–197.
- Andersland, O.B., Ladanyi, B., 2004. Frozen Ground Engineering, , 2nd ed39. The American Society of Civil Engineers and John Wiley and Sons, Inc, Hoboken, New Jersey. https://doi.org/10.1017/S003224740529441X.
- Anderson, D.M., Tice, A.R., 1972. Predicting unfrozen water contents in frozen soils from surface area measurements. Highw. Res. Rec. 393, 12–18.
- Anisimov, O.A., Shiklomanov, N.I., Nelson, F.E., 1997. Global warming and active-layer thickness: results from transient general circulation models. Glob. Planet. Chang. 15 (3–4), 61–77. https://doi.org/10.1016/S0921-8181(97)00009-X.
- Aré, F.E., 1988. Thermal abrasion of sea coasts (part I). Polar Geogr. Geol 12, 1–157. https://doi.org/10.1080/10889378809377343.
- Arenson, L.U., Sego, D.C., 2006. The effect of salinity on the freezing of coarse-grained sands. Can. Geotech. J. 43 (3), 325–337. https://doi.org/10.1139/t06-006.
- Arenson, L.U., Springman, S.M., 2005. Triaxial constant stress and constant strain rate tests on ice-rich permafrost samples. Can. Geotech. J. 42 (2), 412–430. https://doi. org/10.1139/f04-111.
- Arenson, L.U., Springman, S.M., Sego, D.C., 2007. The rheology of frozen soils. Appl. Rheol. 17 (1) https://doi.org/10.1515/arh-2007-0003, 12147-1-12147-14.
- Barkovskaya, Y.N., Yershov, E.D., Kamarove, I.A., Cheveriov, V.G., 1983. Mechansism and regularities of changes in heat conductivity of soils during the freezing-thawing process. In: Proceedings of Fourth International Conference on Permafrost. National Academy Press, Washington, D.C, pp. 46–50.
- Biskaborn, B.K., Smith, S.L., Noetzli, J., Matthes, H., Vieira, G., Streletskiy, D.A., Schoeneich, P., Romanovsky, V.E., Lewkowicz, A.G., Abramov, A., Allard, M., Boike, J., Cable, W.L., Christiansen, H.H., Delaloye, R., Diekmann, B., Drozdov, D., Etzelmüller, B., Grosse, G., Guglielmin, M., Ingeman-Nielsen, T., Isaksen, K., Ishikawa, M., Johansson, M., Johannsson, H., Joo, A., Kaverin, D., Kholodov, A., Konstantinov, P., Kröger, T., Lambiel, C., Lanckman, J.P., Luo, D., Malkova, G., Meiklejohn, I., Moskalenko, N., Oliva, M., Phillips, M., Ramos, M., Sannel, A.B.K., Sergeev, D., Seybold, C., Skryabin, P., Vasiliev, A., Wu, Q., Yoshikawa, K., Zheleznyak, M., Lantuit, H., 2019. Permafrost is warming at a global scale. Nat. Commun. 10 (1), 1–11. https://doi.org/10.1038/s41467-018-08240-4.

- Bronen, R., 2015. Climate-induced community relocations: using integrated social-ecological assessments to foster adaptation and resilience. Ecol. Soc. 20 (3), 36. https://doi.org/10.5751/ES-07801-200336.
- Bronen, R., Chapin, F.S., 2013. Adaptive governance and institutional strategies for climate-induced community relocations in Alaska. Proc. Natl. Acad. Sci. 110 (23), 9320–9325. https://doi.org/10.1073/pnas.1210508110.
- Bronen, R., Pollock, D., Overbeck, J., Stevens, D., Natali, S., Maio, C., 2019. Usteq: integrating indigenous knowledge and social and physical sciences to coproduce knowledge and support community-based adaptation. Polar Geogr. 1–18 https://doi.org/10.1080/1088937X.2019.1679271.
- Chamberlain, E., Groves, C., Perham, R., 1972. The mechanical behaviour of frozen earth materials under high pressure triaxial test conditions. Geotechnique 22 (3), 469–483. https://doi.org/10.1680/geot.1972.22.3.469.
- Christ, M., Kim, Y.C., Park, J.B., 2009. The influence of temperature and cycles on acoustic and mechanical properties of frozen soils. KSCE J. Civ. Eng. 13 (3), 153–159. https://doi.org/10.1007/s12205-009-0153-1.
- Collett, T.S., Bird, K.J., 1988. Freezing-point depression at the base of ice-bearing permafrost on the North Slope of Alaska. In: Proceedings of Fifth International Conference on Permafrost. Tapir Publ Trondheim, Norway, pp. 50–57.
- Costard, F., Dupeyrat, L., Séjourné, A., Bouchard, F., Fedorov, A., Saint-Bézar, B., 2021. Retrogressive thaw slumps on ice-rich permafrost under degradation: results from a large-scale laboratory simulation. Geophys. Res. Lett. 48 (1), e2020GL091070 https://doi.org/10.1029/2020GL091070.
- Crowther, G.S., 1992. Estimating thaw-strain settlement of frozen fill. J. Cold Reg. Eng. 6 (4), 152–159. https://doi.org/10.1061/(ASCE)0887-381X(1992)6:4(152).
- De Guzman, E.M.B., Stafford, D., Alfaro, M.C., Doré, G., Arenson, L.U., 2018. Large-scale direct shear testing of compacted frozen soil under freezing and thawing conditions. Cold Reg. Sci. Technol. 151, 138–147. https://doi.org/10.1016/j. coldregions.2018.03.011.
- Ding, J., 1083. Study and practice on deep foundations in permafrost areas of China. In: Proceedings of Fourth International Conference of Permafrost. National Academy Press, Washington, D.C, pp. 18–24.
- Dumais, S., Konrad, J.M., 2018. One-dimensional large-strain thaw consolidation using nonlinear effective stress-void ratio-hydraulic conductivity relationships. Can. Geotech. J. 55 (3), 414–426. https://doi.org/10.1139/cgj-2017-0221.
- Esch, D.C., 1983. Design and performance of road and railway embankments on permafrost. In: In Proceedings of Fourth International Conference on Permafrost, National Academy Press Washington, D.C., 2, pp. 25–30.
- Ford, J., Pearce, T., Smit, B., Wandel, J., Allurut, M., Shappa, K., Ittusujurat, H., Qrunnut, K., 2007. Reducing vulnerability to climate change in the Arctic: the case of Nunavut, Canada. Arctic 150–166.
- Fu, R., Zhang, J., Hou, Z., 1983. Ultrasonic velocity in frozen soil. In: Proceedings of Fourth International Conference on Permafrost. National Academy Press, Washington, D.C, pp. 311–315.
- Furuberg, T., Berggren, A.L., 1988. Mechanical properties of frozen saline clays. In: Proceedings of Fifth International Conference on Permafrost, Trodheim, Norway, 2, pp. 1078–1084.
- Ge, X., Yang, Z., Still, B., Li, Q., 2012. Experimental study of frozen soil mechanical properties for seismic design of pile foundations. In: Cold Regions Engineering 2012: Sustainable Infrastructure Development in a Changing Cold Environment, pp. 478–488. https://doi.org/10.1061/9780784412473.047.
- Ge, X., Yang, Z., Still, B., 2013. Mechanical properties of naturally frozen ice-rich silty soils. In: Mechanical Properties of Frozen Soil. ASTM International, West Conshohocken, Pennsylvania. https://doi.org/10.1520/STP156820130002.
- Gregersen, O., Phukan, A., Johansen, T., 1983. Engineering properties and foundation design alternatives in marine Svea clay, Svalbard. In: Proceedings of Fourth International Conference on Permafrost. National Academy Press, Washington, D.C, pp. 384–388.
- Hanna, A.J., McRoberts, E.C., 1988. Permafrost slope design for a buried oil pipeline. In: Proceedings of Fifth International Conference on Permafrost, Trondheim, Norway, 2, pp. 1247–1252.
- Hansson, K., Šimůnek, J., Mizoguchi, M., Lundin, L.C., Van Genuchten, M.T., 2004.
 Water flow and heat transport in frozen soil: Numerical solution and freeze-thaw applications. Vadose Zone J. 3 (2), 693–704. https://doi.org/10.2113/3.2.693.
- Heuer, C.E., Caldwell, J.B., Zamsky, B., 1983. Design of buried seafloor pipelines for permafrost thaw settlement. In: Proceedings of the Fourth International Conference on Permafrost, Fairbanks, Alaska, pp. 486–491.
- Hjort, J., Karjalainen, O., Aalto, J., Westermann, S., Romanovsky, V.E., Nelson, F.E., Etzelmüller, B., Luoto, M., 2018. Degrading permafrost puts Arctic infrastructure at risk by mid-century. Nat. Commun. 9 (1), 5147. https://doi.org/10.1038/s41467-018-07557-4.
- Hoekstra, P., 1966. Moisture movement in soils under temperature gradients with the cold-side temperature below freezing. Water Resour. Res. 2 (2), 241–250. https:// doi.org/10.1029/WR002i002p00241.
- Hollesen, J., Callanan, M., Dawson, T., Fenger-Nielsen, R., Friesen, T.M., Jensen, A.M., Markham, A., Martens, V.V., Pitulko, V.V., Rockman, M., 2018. Climate change and the deteriorating archaeological and environmental archives of the Arctic. Antiquity 92 (363), 573–586. https://doi.org/10.15184/aqy.2018.8.
- Hoque, M.A., Pollard, W.H., 2009. Arctic coastal retreat through block failure. Can. Geotech. J. 46 (10), 1103–1115. https://doi.org/10.1139/T09-058.
- Hoque, M.A., Pollard, W.H., 2016. Stability of permafrost dominated coastal cliffs in the Arctic. Polar Sci. 10 (1), 79–88. https://doi.org/10.1016/j.polar.2015.10.004.
- Hui, B., Ping, H., 2009. Frost heave and dry density changes during cyclic freeze-thaw of a silty clay. Permafr. Periglac. Process. 20 (1), 65–70. https://doi.org/10.1002/ ppp.636.

- Jessberger, H.L., 1980. Theory and application of ground freezing in civil engineering. Cold Reg. Sci. Technol. 3 (1), 3–27. https://doi.org/10.1016/0165-232X(80)90003-
- Jessberger, H.L., 1981. A state-of-the-art report. Ground freezing: mechanical properties, processes and design. Eng. Geol. 29, 5–30. https://doi.org/10.1016/B978-0-444-42010-7.50006-2.
- Jorgenson, M.T., Shur, Y.L., Pullman, E.R., 2006. Abrupt increase in permafrost degradation in Arctic Alaska. Geophys. Res. Lett. 33 (2), L02503. https://doi.org/ 10.1029/2005GL024960.
- Kadivar, M., Manahiloh, K.N., 2019. Revisiting parameters that dictate the mechanical behavior of frozen soils. Cold Reg. Sci. Technol. 163, 34–43. https://doi.org/ 10.1016/j.coldregions.2019.04.005.
- Kanevskiy, M., Shur, Y., Connor, B., Dillon, M., Stephani, E., O'Donnell, J., 2012. Study of the ice-rich syngenetic permafrost for road design (Interior Alaska). In: Proceedings of the Tenth International Conference on Permafrost, Salekhard, Russia, np. 191–196.
- Kim, Y., Chae, D., Kim, K., Cho, W., 2015. Physical and mechanical characteristics of frozen ground at various sub-zero temperatures. KSCE J. Civ. Eng. 20 (6), 2365–2374. https://doi.org/10.1007/s12205-015-0542-6.
- Ladanyi, B., 1972. An engineering theory of creep of frozen soils. Can. Geotech. J. 9 (1), 63–80. https://doi.org/10.1139/t72-005.
- Ladanyi, B., 1981. Mechanical behavior of frozen soils. In: Selvadurai, A.P.S. (Ed.), Mechanics of Structured Media, Proceedings of the International Symposium on the Mechanical Behaviour of Structured Media, Ottawa, Ont., 18–21 May 1981. Elsevier, New York, pp. 205–245.
- Lantuit, H., Pollard, W.H., 2008. Fifty years of coastal erosion and retrogressive thaw slump activity on Herschel Island, southern Beaufort Sea, Yukon Territory, Canada. Geomorphology 95 (1–2), 84–102. https://doi.org/10.1016/j. geomorph.2006.07.040.
- Larsen, P.H., Goldsmith, S., Smith, O., Wilson, M.L., Strzepek, K., Chinowsky, P., Saylor, B., 2008. Estimating future costs for Alaska public infrastructure at risk from climate change. Glob. Environ. Chang. 18 (3), 442–457. https://doi.org/10.1016/j. gloenycha.2008.03.005.
- Lee, M.Y., Fossum, A., Costin, L.S., Bronowski, D., 2002. Frozen soil material testing and constitutive modeling. Sandia Report, Albuquerque, New Mexico 524, 8–65. https:// doi.org/10.2172/793403.
- Li, H., 2009. Experimental and Numerical Study of Sonic Wave Propagation in Freezing Sand and Silt. Doctoral Dissertation. University of Alaska Fairbanks, Fairbanks, Alaska.
- Li, Z., Chen, J., Sugimoto, M., 2020. Pulsed NMR measurements of unfrozen water content in partially frozen soil. J. Cold Reg. Eng. 34 (3), 04020013. https://doi.org/ 10.1061/(ASCE)CR.1943-5495.0000220.
- Liew, M., Xiao, M., Jones, B.M., Farquharson, L.M., Romanovsky, V.E., 2020. Prevention and control measures for coastal erosion in northern high-latitude communities: a systematic review based on Alaskan case studies. Environ. Res. Lett. 15 (9), 093002 https://doi.org/10.1088/1748-9326/ab9387.
- Liu, L., Zhao, D., Wei, J., Zhuang, Q., Gao, X., Zhu, Y., Zhang, J., Guo, C., Zheng, D., 2021. Permafrost sensitivity to global warming of 1.5°C and 2°C in the Northern Hemisphere. Environ. Res. Lett. 16 (3), 034038 https://doi.org/10.1088/1748-0325 (ab.)4602
- Luo, D., Jin, H., Marchenko, S.S., Romanovsky, V.E., 2018. Difference between near-surface air, land surface and ground surface temperatures and their influences on the frozen ground on the Qinghai-Tibet Plateau. Geoderma 312 (2018), 74–85. https://doi.org/10.1016/j.geoderma.2017.09.037.
- Ma, W., Wu, Z., Zhang, C., 1993. Strength and yield criteria of frozen soil. In: Proceedings of the Sixth International Conference on Permafrost. Beijing. China. pp. 432–435.
- Mageau, D.W., Morgenstern, N.R., 1980. Observations on moisture migration in frozen soils. Can. Geotech. J. 17 (1), 54–60. https://doi.org/10.1139/t80-005.
- Maldonado, J.K., Shearer, C., Bronen, R., Peterson, K., Lazrus, H., 2013. The impact of climate change on tribal communities in the US: displacement, relocation, and human rights. In: Climate Change and Indigenous Peoples in the United States. Springer, Cham, pp. 93–106. https://doi.org/10.1007/978-3-319-05266-3_8.
- Marino, E., 2012. The long history of environmental migration: assessing vulnerability construction and obstacles to successful relocation in Shishmaref, Alaska. Glob. Environ. Chang. 22 (2), 374–381. https://doi.org/10.1016/j. gloenvcha.2011.09.016.
- Marsadolov, L.S., Paranina, A.N., Grigoryev, A.A., Sukhorukov, V.D., 2019. Problems of preservation of prehistoric cultural heritage objects in the Arctic. In: Proceedings of Fourth International Scientific Conference Arctic: History and Modernity, St. Petersburg, Russia, 302. IOP Publishing, p. 012149. https://doi.org/10.1088/1755-1315/302/1/012149 (1).
- Mavko, G., Mukerji, T., Dvorkin, J., 2003. The Rock Physics Handbook. Cambridge University Press, Cambridge, United Kingdom. https://doi.org/10.1017/ CB09780511626753.
- McGaw, R.W., Berg, R.L., Ingersoll, J.W., 1983. An investigation of transient processes in an advancing zone of freezing. In: Proceedings of Fourth International Conference on Permafrost, Washington, D.C, pp. 821–825.
- Melvin, A.M., Larsen, P., Boehlert, B., Neumann, J.E., Chinowsky, P., Espinet, X., Martinich, J., Baumann, M.S., Rennels, L., Bothner, A., Nicolsky, D.J., Marchenko, S. S., 2016. Climate change damages to Alaska public infrastructure and the economics of proactive adaptation. Proc. Natl. Acad. Sci. 114 (2), E122–E131. https://doi.org/ 10.1073/pnas.1611056113.
- Meng, Q., Li, D., Chen, J., Xu, A., Huang, S., 2008. Experimental research on physical-mechanical characteristics of frozen soil based on ultrasonic technique. In: Proceedings of Ninth International Conference on Permafrost, Fairbanks, Alaska, 2, pp. 1179–1183.

- Morgenstern, N.R., 1983. Deep foundations and embankments introduction. In:

 Proceedings of the Fourth International Conference of Permafrost, Washington, D.C.,
 p. 15
- Morgenstern, N.T., Nixon, J.F., 1971. One-dimensional consolidation of thawing soils. Can. Geotech. J. 8 (4), 558–565. https://doi.org/10.1139/t71-057.
- Nakano, Y., Arnold, R., 1973. Acoustic properties of frozen Ottawa sand. Water Resour. Res. 9 (1), 178–184. https://doi.org/10.1029/WR009i001p00178.
- Nash, A., Carlson, A.R., 2015. Permafrost: A Building Problem in Alaska. University of Alaska Fairbanks Cooperative Extension Service, Alaska, pp. 1–4.
- Nelson, R.A., Luscher, U., Rooney, J.W., Stramler, A.A., 1983. Thaw strain data and thaw settlement predictions for alaskan soils. In: Proceedings of the Fourth International Conference on Permafrost, Fairbanks, Alaska, pp. 912–917.
- Nelson, F.E., Anisimov, O.A., Shiklomanov, N.I., 2001. Subsidence risk from thawing permafrost. Nature 410 (6831), 889. https://doi.org/10.1038/35073746.
- Nelson, F.E., Anisimov, O.A., Shiklomanov, N.I., 2002. Climate change and hazard zonation in the circum-Arctic permafrost regions. Nat. Hazards 26 (3), 203–225. https://doi.org/10.1023/A:1015612918401.
- Nicolsky, D.J., Romanovsky, V.E., 2018. Modeling long-term permafrost degradation. J. Geophys. Res. Earth Surf. 123, 1756–1771. https://doi.org/10.1029/ 2018JF004655.
- Oliphant, J.L., Tice, A.R., Nakano, Y., 1983. Water migration due to a temperature gradient in frozen soil. In: Proceedings of Fourth International Conference on Permafrost, Washington, D.C, pp. 951–956.
- Olsen, J.R. ed, 2015. Adapting Infrastructure and Civil Engineering Practice to a Changing Climate. American Society of Civil Engineers, Reston, Virginia. https://doi.org/10.1061/9780784479193.
- Osterkamp, T.E., 2007. Characteristics of the recent warming of permafrost in Alaska.

 J. Geophys. Res. Earth Surf. 112, F02S02. https://doi.org/10.1029/2006JF000578.
- Osterkamp, T.E., Romanovsky, V.E., 1999. Evidence for warming and thawing of discontinuous permafrost in Alaska. Permafr. Periglac. Process. 10 (1), 17–37. https://doi.org/10.1002/(SICI)1099-1530(199901/03)10:1<17::AID-PPP303>3.0. CO;2-4.
- Overduin, P.P., Strzelecki, M.C., Grigoriev, M.N., Couture, N., Lantuit, H., St-Hilaire-Gravel, D., Günther, F., Wetterich, S., 2014. Coastal changes in the Arctic. Geol. Soc. Lond., Spec. Publ. 388 (1), 103–129. https://doi.org/10.1144/SP388.13.
- Parameswaran, V.R., Jones, S.J., 1981. Triaxial testing of frozen sand. J. Glaciol. 27 (95), 147–155. https://doi.org/10.1017/S0022143000011308.
- Parazoo, N.C., Koven, C.D., Lawrence, D.M., Romanovsky, V., Miller, C.E., 2018. Detecting the permafrost carbon feedback: Talik formation and increased cold-season respiration as precursors to sink-to-source transitions. Cryosphere 12 (1), 123–144. https://doi.org/10.5194/tc-12-123-2018.
- Pierce, J., Williams, G., Simpson, T.W., Meisel, N.A., McComb, C., 2021. Stochastically-trained physics-informed neural networks: Application to thermal analysis in metal laser powder bed fusion. In: Proceedings of the ASME 2021, International Design Engineering Technical Conference and Computers and Information in Engineering Conference, virtual.
- Pullman, E.R., Torre Jorgenson, M., Shur, Y., 2007. Thaw settlement in soils of the Arctic Coastal Plain, Alaska. Arct. Antarct. Alp. Res. 39 (3), 468–476. https://doi.org/10.1657/1523-0430(05-045)[PULLMAN]2.0.CO:2.
- Qi, J., Vermeer, P.A., Cheng, G., 2006. A review of the influence of freeze-thaw cycles on soil geotechnical properties. Permafr. Periglac. Proces. 17 (3), 245–252. https://doi. org/10.1002/ppp.559.
- Qi, J., Wang, S., Yu, F., 2013. A review on creep of frozen soils. In: Constitutive Modeling of Geomaterials. Springer, Berlin, Heidelberg, pp. 129–133. https://doi.org/ 10.1007/978-3-642-32814-5 13.
- Razbegin, V.N., Vyalov, S.S., Maksimyak, R.V., Sadovskii, A.V., 1996. Mechanical properties of frozen soils. Soil Mech. Found. Eng. 33 (2), 35–45. https://doi.org/ 10.1007/BF02354292.
- Rempel, A.W., 2007. Formation of ice lenses and frost heave. J. Geophys. Res. Earth Surf. 112 (F02S21) https://doi.org/10.1029/2006JF000525.
- Rice, E.F., 1972. Building in the North. Geophysical Institute of the University of Alaska, Fairbanks.
- Riseborough, D.W., Smith, M.W., Halliwell, D.H., 1983. Determination of the thermal properties of frozen soils. In: Proceedings of Fourth International Conference on Permafrost, Washington, D.C, pp. 1072–1077.
- Romanovsky, V.E., Osterkamp, T.E., 2000. Effects of unfrozen water on heat and mass transport processes in the active layer and permafrost. Permafr. Periglac. Process. 11 (3), 219–239. https://doi.org/10.1002/1099-1530(200007/09)11:3<219::AID-PPP352>3.0.C0:2-7.
- Romanovsky, V.E., Smith, S.L., Christiansen, H.H., 2010. Permafrost thermal state in the polar northern hemisphere during the international polar year 2007–2009: *a* synthesis. Permafr. Periglac. Process. 21, 106–116. https://doi.org/10.1002/
- Roth, K., Boike, J., 2001. Quantifying the thermal dynamics of a permafrost site near Ny-Ålesund, Svalbard. Water Resour. Res. 37 (12), 2901–2914. https://doi.org/ 10.1029/2000WR000163.
- Rowland, J.C., Jones, C.E., Altmann, G., Bryan, R., Crosby, B.T., Hinzman, L.D., Kane, D. L., Lawrence, D.M., Mancino, A., Marsh, P., McNamara, J.P., 2010. Arctic landscapes in transition: responses to thawing permafrost. EOS Trans. Am. Geophys. Union 91 (26), 229–230. https://doi.org/10.1029/2010EO260001.
- Sayles, F.H., 1974. Triaxial constant strain rate tests and triaxial creep tests on frozen Ottawa sand (no. 253). In: Corps of Engineers, US Army Cold Regions Research and Engineering Laboratory, Technical Report 253, Hanover, New Hampshire.
- Sayles, F.H., 1983. Design and performance of water-retaining embankments in permafrost. In: Proceedings of Second International Conference on Permafrost, Fairbanks, Alaska, pp. 31–42.

- Shearer, C., 2012. The political ecology of climate adaptation assistance: Alaska natives, displacement, and relocation. J. Politic. Ecol. 19 (2012), 174–183. https://doi.org/ 10.2458/v1911.21725
- Shelman, A., Tantalla, J., Sritharan, S., Nikolaou, S., Lacy, H., 2014. Characterization of seasonally frozen soils for seismic design of foundations. J. Geotech. Geoenviron. 140 (7), 04014031. https://doi.org/10.1061/(ASCE)GT.1943-5606.0001065.
- Smith, S.L., Riseborough, D.W., 2010. Modelling the thermal response of permafrost terrain to right-of-way disturbance and climate warming. Cold Reg. Sci. Technol. 60 (1), 92–103. https://doi.org/10.1016/j.coldregions.2009.08.009.
- Smith, M.W., Tice, A.R., 1988. Measurement of the unfrozen water content of soils. In: Comparison of NMR (Nuclear Magnetic Resonance) and TDR (Time Domain Reflectometry) Methods. New Hampshire, Cold Regions Research and Engineering Lab Hanover
- Tang, L., Wang, X., Lan, F., Qiu, P., Jin, L., 2020. Measuring the content of unfrozen water in frozen soil based on resistivity. Int. J. Electrochem. Sci. 15, 9459–9472. https://doi.org/10.20964/2020.09.57.
- Thomas, H.R., Cleall, P., Li, Y.C., Harris, C., Kern-Luetschg, M., 2009. Modelling of cryogenic processes in permafrost and seasonally frozen soils. Geotechnique 59 (3), 173–184. https://doi.org/10.1680/geot.2009.59.3.173.
- Tian, Y., Yang, Z.J., Tai, B., Li, Y., Shen, Y., 2019. Damage and mitigation of railway embankment drainage trench in warm permafrost: a case study. Eng. Geol. 261, 105276 https://doi.org/10.1016/j.enggeo.2019.105276.
- Ting, J.M., 1983. Tertiary creep model for frozen sands. J. Geotech. Eng. 109 (7), 932–945. https://doi.org/10.1061/(ASCE)0733-9410(1983)109:7(932).
- Ting, J.M., Torrence Martin, R., Ladd, C.C., 1983. Mechanisms of strength for frozen sand. J. Geotech. Eng. 109 (10), 1286–1302. https://doi.org/10.1061/(ASCE)0733-9410(1983)109:10(1286).
- Tong, Z., 1983. In-situ direct shear tests at the freeze/thaw interface and in thawed soils. In: Proceedings of Fourth International Conference on Permafrost, Washington, D.C, pp. 1278–1282.
- U.S. Arctic Research Commission Permafrost Task Force, 2003. Climate Change, Permafrost, and Impacts on Civil Infrastructure. In: Special Report 01–03. Arctic Research Commission, Arlington, Virginia, U.S.
- Vyalov, S.S., 1983. Placing of deep pile foundations in permafrost in the USSR. In: Proceedings of Fourth International Conference of Permafrost, Washington, D.C, pp. 16–17.

- Wang, D.W., Zhu, Y.L., Ma, W., Niu, Y.H., 2006. Application of ultrasonic technology for physical-mechanical properties of frozen soils. Cold Reg. Sci. Technol. 44, 12–19. https://doi.org/10.1016/j.coldregions.2005.06.003.
- Weaver, J.S., Morgenstern, N.R., 1981. Pile design in permafrost. Can. Geotech. J. 18 (3), 357–370. https://doi.org/10.1139/t81-043.
- Williams, P.J., 1964. Unfrozen water content of frozen soils and soil moisture suction. Geotechnique 14 (3), 231–246. https://doi.org/10.1680/geot.1964.14.3.231.
- Williams, P.J., Smith, M.W., 1989. The Frozen Earth: Fundamentals of Geocryology. Cambridge University Press, Cambridge, p. 306.
- Yamamoto, Y., 2013. Instabilities in Alpine Permafrost: Strength and Stiffness in a Warming Regime. Dissertation. Swiss Federal Institute of Technology Zürich, Zürich, Switzerland.
- Yang, Z., Ge, X., Still, B., Paris, A., 2012. Frozen Soil Lateral Resistance for the Seismic Design of Highway Bridge Foundations. Alaska University Transportation Center, Alaska Department of Transportation and Public Facilities, Fairbanks, Alaska.
- Yang, Z.J., Still, B., Ge, X., 2015. Mechanical properties of seasonally frozen and permafrost soils at high strain rate. Cold Reg. Sci. Technol. 113, 12–19. https://doi. org/10.1016/j.coldregions.2015.02.008.
- Zhang, Y., Michalowski, R.L., 2015. Thermal-hydro-mechanical analysis of frost heave and thaw settlement. J. Geotech. Geoenviron. 141 (7), 04015027. https://doi.org/ 10.1061/(ASCE)GT.1943-5606.0001305.
- Zhang, L., Ma, W., Yang, C., Wen, Z., Dong, S., 2016. An investigation of pore water pressure and consolidation phenomenon in the unfrozen zone during soil freezing. Cold Reg. Sci. Technol. 130, 21–32. https://doi.org/10.1016/j. coldregions.2016.07.007.
- Zhang, D., Liu, E., Liu, X., Zhang, G., Song, B., 2017. A new strength criterion for frozen soils considering the influence of temperature and coarse-grained contents. Cold Reg. Sci. Technol. 143, 1–12. https://doi.org/10.1016/j.coldregions.2017.08.006.
- Zhang, F., Yang, Z., Still, B., Wang, J., Yu, H., Zubeck, H., Petersen, T., Aleshire, L., 2018. Elastic properties of saline permafrost during thawing by bender elements and bending disks. Cold Reg. Sci. Technol. 146, 60–71. https://doi.org/10.1016/j. coldregions.2017.11.014.
- Zhu, Y., Carbee, D.L., 1988. Triaxial compressive strength of frozen soils under constant strain rates. In: Proceedings of the Fifth International Conference on Permafrost, Trondheim, Norway, 2, pp. 1200–1206.
- Zimmerman, R.W., King, M.S., 1986. The effect of the extent of freezing on seismic velocities in unconsolidated permafrost. Geophysics 51 (6), 1285–1290. https://doi. org/10.1190/1.1442181.